Published in final edited form as:
Neuroscience. 2007 July 29; 147(4): 938–956.

Identification of connexin36 in gap junctions between neurons in rodent locus coeruleus

J.E. Rash[1,2], **C.O. Olson**[3], **K.G.V. Davidson**[1], **T. Yasumura**[1], **N. Kamasawa**[1,*], and **J.I. Nagy**[3]

1*Department of Biomedical Sciences, Colorado State University, Fort Collins, CO 80523, USA*

2*Department of Program in Molecular, Cellular and Integrative Neurosciences, Colorado State University, Fort Collins, CO 80523, USA*

3*Department of Physiology, Faculty of Medicine, University of Manitoba, Winnipeg, Manitoba R3E 3J7, Canada*

Abstract

Locus coeruleus neurons are strongly coupled during early postnatal development, and it has been proposed that these neurons are linked by extraordinarily abundant gap junctions consisting of connexin32 and connexin26, and that those same connexins abundantly link neurons to astrocytes. Based on the controversial nature of those claims, immunofluorescence imaging and freeze-fracture replica immunogold labeling were used to re-investigate the abundance and connexin composition of neuronal and glial gap junctions in developing and adult rat and mouse locus coeruleus. In early postnatal development, connexin36 and Cx43 immunofluorescent puncta were densely distributed in the locus coeruleus, whereas connexin32 and connexin26 were not detected. By freeze-fracture replica immunogold labeling, connexin36 was found in ultrastructurally-defined neuronal gap junctions, whereas connexin32 and connexin26 were not detected in neurons and only rarely detected in glia. In 28-day postnatal (adult) rat locus coeruleus, immunofluorescence labeling for connexin26 was always co-localized with the glial gap junction marker connexin43; connexin32 was associated with the oligodendrocyte marker CNPase; and connexin36 was never co-localized with connexin26, Cx32 or connexin43. Ultrastructurally, connexin36 was localized to gap junctions between neurons, whereas connexin32 was detected only in oligodendrocyte gap junctions; and Cx26 was found only rarely in astrocyte junctions but abundantly in pia mater. Thus, in developing and adult locus coeruleus, neuronal gap junctions contain connexin36 but do not contain detectable connexin32 or connexin26, suggesting that the locus coeruleus has the same cell-type specificity of connexin expression as observed ultrastructurally in other regions of the central nervous system. Moreover, in both developing and adult locus coeruleus, no evidence was found for gap junctions or connexins linking neurons with astrocytes or oligodendrocytes, indicating that neurons in this nucleus are not linked to the pan-glial syncytium by connexin32- or connexin26-containing gap junctions or by abundant free connexons composed of those connexins.

Keywords

astrocytes; connexin26; connexin32; connexin43; oligodendrocytes

Corresponding author: Dr. J.E. Rash Email: john.rash@colostate.edu Department of Biomedical Sciences Colorado State University, Campus delivery 1617, Fort Collins, Colorado USA, 80523 Phone: (970) 491−5606 Fax: (970) 491−7907
*Current address: Division of Cerebral Structure, National Institute of Physiological Sciences, Okazaki 444−8787, Japan

In the developing mammalian central nervous system (CNS), electrical coupling between neurons is well documented by electrophysiological and dye-coupling approaches (Peinado et al., 1993;Fulton, 1995;Montoro and Yuste, 2004;Bruzzone and Dermietzel, 2006). In recent years, sensitive electrophysiological techniques have also documented electrical synapses in numerous adult brain regions (Bennett and Zukin, 2004); mRNA for the gap junction protein connexin36 (Cx36) was widely detected in neurons but not glia (Condorelli et al., 1998;Condorelli et al., 2000); and Cx36 was found to be present in ultrastructurally-defined gap junctions between neurons in many regions of both developing and adult CNS (Rash et al., 2001b;Nagy et al., 2004;Li et al., 2004a;Rash et al., 2005;Kamasawa et al., 2006;Fukuda et al., 2006). Moreover, the functional importance of Cx36 in adult brain is indicated by deficits in neuronal network properties and by behavioral impairments in Cx36 knockout mice (Hormuzdi et al., 2004;Frisch et al., 2005).

Neurons of the locus coeruleus (LC) in rats have synchronized rhythmic electrical oscillations during early postnatal development, correlated with substantial electrical and dye-coupling between pairs of neurons (Christie et al., 1989;Christie and Jelinek, 1993;Oyamada et al., 1999;Andrzejewski et al., 2001;Ballantyne et al., 2004). In addition, synchronous electrical activity of LC neurons has been observed in slices from adult rats under conditions that indirectly support mediation of this activity by gap junctional coupling (Travagli et al., 1995;Ishimatsu and Williams, 1996;Alvarez et al., 2002). *In vivo*, synchronized LC neuronal activity may have functional impact by promoting synchronous release of norepinephrine throughout the widespread projection areas of the LC, which is thought to contribute to overall cognitive performance, learning and memory (Ashton-Jones and Cohen, 2005,2006). In addition to coupling between LC neurons, recent studies (Alvarez-Maubecin et al., 2000;Van Bockstaele et al., 2004) suggested widespread but weak gap junctional coupling between LC neurons and astrocytes in neonatal and adult rats, including strong dye-transfer from astrocytes to some neurons. Using silver-intensified immunogold-labeling electron microscopic immunocytochemistry, they described detection of connexin32 (Cx32) and connexin26 (Cx26) protein in a very high percentage of dendro-dendritic profiles and proposed even greater abundance of these two connexins at membrane appositions between dendrites and glial cells (primarily astrocytes).

While clear evidence exists for coupling between neurons in developing LC, several challenging issues remain concerning documentation of gap junctional coupling in this nucleus: **1)** No ultrastructural data exist for the presence of connexin-containing membrane appositions between neurons in the LC that meet accepted criteria for designation as gap junctions (Brightman and Reese, 1969;Sotelo and Korn, 1978;Rash et al., 1998); **2)** Unlike the reported expression of abundant Cx26 and Cx32 in both neurons and astrocytes in LC, all other locations in the CNS examined by freeze-fracture replica immunolabeling (FRIL) electron microscopy have revealed cell-type-specific expression of connexin proteins, with Cx32 found only in gap junctions formed by oligodendrocytes (Rash et al., 2001a;Nagy et al., 2003a;Li et al., 2004a;Kamasawa et al., 2005), Cx26 only in gap junctions formed by pia mater and by subpopulations of astrocytes [(Nagy et al., 2001,2003b;Rash et al., 2001a); also see Mercier and Hatton (2001) and Altevogt et al., (2004)], and Cx36 only in neuronal gap junctions (Rash et al., 2000,2001b,2005;Kamasawa et al., 2006) [also see Fukuda et al. (2006)]; **3)** Although proposals for coupling of neurons to astrocytes based on propagation of “calcium waves” (Nedergaard, 1994) were extended to dye coupling between astrocytes and neurons in LC slice preparations (Alvarez-Maubecin et al., 2000;Van Bockstaele et al., 2004), other non-gap-junctional mechanisms appear to account for initiation and propagation of calcium waves (Charles, 1994,1996;Parpura et al., 1994;Hassinger et al., 1995); and **4)** Despite extensive studies of numerous brain regions (Brightman and Reese, 1969;Sotelo and Korn, 1978;Kosaka, 1985;Rash et al., 1998,2001b;Kosaka and Kosaka, 2005), no ultrastructural evidence has been

found for the existence of neuron-to-astrocyte gap junctions. These divergent reports raise questions about the reported uniqueness of the LC, particularly during development, with respect to the abundance and connexin composition of its neuronal gap junctions and to the occurrence of neuronal/glial gap junctions. In view of these issues, we investigated Cx26, Cx32 and Cx36 distribution in the LC of neonatal and adult rats and mice by immunofluorescence microscopy and FRIL, with localization of two additional connexins, Cx43 and Cx47, used to support assignment of cell identities.

EXPERIMENTAL PROCEDURES

Animals

All animals used in this study were prepared under protocols approved by the Institutional Animal Care and Use Committees of Colorado State University and the University of Manitoba, and were conducted according to the *Principles of Laboratory Animal Care* (NIH publication No. 80−23, Rev. 1996). These protocols included minimization of stress to animals and minimization of number of animals used. For light microscopy, six adult male CD1 mice, two adult Cx36 KO C57/BL6 mice, 10 adult male Sprague-Dawley rats, and eight CD1 mice at postnatal day 7 (P7) were obtained from Central Animal Care Services at the University of Manitoba. For FRIL, P7-P21 and adult Sprague-Dawley rats were obtained from Laboratory Animal Services at Colorado State University. In addition, mice whose LC neurons express Enhanced Green Fluorescent Protein (EGFP) (van den Pol et al., 2002) were obtained from a colony established courtesy of Anthony N. van den Pol, Yale University School of Medicine, New Haven, CT.

Light microscope immunohistochemistry

Mice and rats deeply anesthetized with equithesin (3 ml/kg) were transcardially perfused with cold 50 mM sodium phosphate buffer, pH 7.4, containing 0.9% NaCl, 0.1% sodium nitrate and 1 unit/ml heparin, and then further perfused with cold 0.16 M sodium phosphate buffer, pH 7.6, containing 1% or 2% formaldehyde and 0.2% picric acid. The fixative was flushed from animals by perfusion with 25 mM sodium phosphate buffer, pH 7.4, containing 10% sucrose. To reexamine the reported sensitivity of connexin immunolabeling to different fixation conditions (Nagy and Rash, 2000;Nagy et al., 2004), two additional rats were prepared for immunohistochemistry following the protocol of Alvarez-Maucebin et al. (2000): after perfusion of pre-fixative clearing solution, rats were perfused sequentially with fixative containing a mixture of 3.75% acrolein and 2% formaldehyde, followed by perfusion with fixative containing 2% formaldehyde, both in 0.1 M phosphate buffer, pH 7.4. After both fixation protocols, brains were removed and cryoprotected for 24−48 h in the final sucrose-containing perfusate.

Transverse sections were cut at a thickness of 15μm on a cryostat and collected on gelatinized glass slides. Sections were air dried, then washed for 20 min in 50 mM Tris-HCl, pH 7.4, containing 1.5% sodium chloride (TBS) and 0.3% Triton X-100 (TBSTr). For studies of early postnatal brains, P7 rat pups were anesthetized as above, decapitated, and unfixed brains were removed and frozen for cryosectioning. Sections were air dried, then immersed in ice-cold 2% formaldehyde for 5 min, followed by two 5 min washes in 50 mM Tris-HCl buffer, pH 7.4, and washed for 20 min in TBSTr. For single- and double-immunofluorescence labeling, sections were incubated with primary antibodies for 24 h at 4°C, then washed for 1 h in TBSTr, and incubated for 1.5 h at room temperature with appropriate secondary antibodies.

Antibodies.—The primary antibodies used, their sources and dilutions employed are indicated in Table 1. Most of these antibodies were obtained from Invitrogen/Zymed Laboratories (Carlsbad, CA, USA), except mouse monoclonal anti-2,'3'-cyclic nucleotide 3'-

phosphodiesterase (CNPase)(Scherer et al., 1994), which was obtained from Sternberger Monoclonals (Lutherville, MD, USA); rabbit polyclonal anti-tyrosine hydroxylase (TH), which was obtained from Eugene Tech International (Ridgefield Park, NJ, USA); and anti-Cx43 antibody 18A, which was generously provided by E. L Hertzberg (Albert Einstein College of Medicine, New York). Western blotting and immunofluorescence characterization of the antibodies for Cx26, Cx32, Cx36, Cx43 and Cx47 have been described previously (Li et al., 1998, 2004; Nagy et al., 2001,2003a,2003b). In addition, specificity of immunofluorescence labeling with anti-Cx36 39−4200 is shown in the present report.

Secondary antibodies included Cy3-conjugated goat or donkey anti-mouse IgG diluted 1:300 (Jackson ImmunoResearch Laboratories, West Grove, PA, USA), Alexa Flour 488-conjugated goat anti-rabbit IgG diluted 1:1000 (Molecular Probes, Eugene, OR, USA), FITC-conjugated horse anti-mouse IgG diluted 1:100 (Vector Laboratories, Inc., Burlingame, CA, USA) and Cy3-conjugated donkey anti-rabbit IgG diluted 1:200 (Jackson). All antibodies were diluted in TBSTr containing 10% normal goat or normal donkey serum. After secondary antibody incubations, sections were washed in TBSTr for 20 min, then washed in 50 mM Tris-HCl buffer, pH 7.4 for 30 min, covered with antifade medium and coverslipped. Control procedures for double labeling included omission of one of the primary antibodies with inclusion of each of the secondary antibodies. In addition, absence of labeling in Cx36 KO mice established the specificity of immunolabeling for Cx36 observed in the LC of wild-type mice.

Immunofluorescence imaging.—Conventional and confocal immunofluorescence images were acquired on a Zeiss Axioskop2 fluorescence microscope using Axiovision 4.5 software (Carl Zeiss Canada, Toronto, ON, Canada) and on an Olympus Fluoview IX70 confocal microscope using Olympus Fluoview 2.1 software (Olympus Canada, Inc., Markham, ON, Canada), and assembled using Adobe Photoshop CS (Adobe Systems, San Jose, CA, USA), CorelDRAW Graphics Suite 12 (Corel Corporation, Ottawa, ON, Canada), and Northern Eclipse software (Empix Imaging, Mississauga, ON, Canada). For generation of stereoscopic confocal immunofluorescence images of labeling for Cx36 in the locus coeruleus, a z-stack of 33 images taken at 0.4 μm intervals was used to make a stacked projection of the left image. For the right image, the original z-stack was used to generate a second projection having a horizontal offset of 7° from that of the left z-stack projection. The two images form a stereoscopic pair that may be viewed either with crossed eyes or using a parallel-axis stereopticon-type viewer.

Freeze-fracture replica immunogold labeling (FRIL)

Animals; formaldehyde fixation for FRIL.—Five postnatal rats (one P7 male, one P14 female and one P14 male, and two P28 males), and four EGFP-LC mice (three P21 males and one P28 female) were anesthetized with ketamine (90 mg/kg) and xylazine (8 mg/kg) and fixed by transcardiac perfusion with 2%-4% formaldehyde in Sørensen's phosphate buffer (pH 7.4), as detailed previously (Rash and Yasumura, 1999). Immediately following perfusion fixation, the rats were decapitated, consistent with recommendations of the Capital Panel on Euthanasia of the American Veterinary Association. Hindbrains were embedded in gelatin, and sections containing LC, corresponding to plates 56−61 of Paxinos and Watson (1998), were cut into 100-μm-thick slices, and freeze-fracture replicated in a JEOL/RFD 9010C freeze-fracture machine (RMC/Boeckler; USA sales agents for JEOL, Inc., Akishima, Japan), as modified (Rash and Yasumura, 1992;Kamasawa et al., 2006). All samples were prepared by “grid-mapped freeze fracture” (Rash et al., 1995,1996), which involves bonding the frozen replicated tissue to a gold "index" grid using Lexan, followed by thawing and photo-mapping in a Zeiss LSM 510 Meta confocal microscope (Carl Zeiss, Inc., Thornwood, NY). Samples were mapped both in transmitted light and by autofluorescence to reveal the location of the LC with respect to the indexed grid openings. Anatomical locations were confirmed in confocal

immunofluorescence grid-mapped replicas from mice whose LC neurons express EGFP. The locations of mapped LCs were internally verified in most FRIL replicas based on relative proximity to ependymocytes in the lateral margins of the overlying fourth ventricle. Portions of replicas that extended beyond the grid were dissected and remounted on index grid, and the unique shape was used for re-orientation with the original photomap.

Replica cleaning in SDS and immunogold labeling.—After photomapping, samples were washed for ca. 29 h at 48°-50°C in 2.5% SDS detergent (Fujimoto, 1995), and sites of non-specific binding to the highly adsorbent platinum and carbon layers of the replica (Dinchuk et al., 1987;Rash et al., 1989;Fujimoto, 1995) were blocked in a solution of 1.5% fish gelatin digest plus 10% heat inactivated goat serum (both from Sigma-Aldrich, St. Louis, MO) (Dinchuk et al., 1987) in Sørensen's phosphate buffer. Replicas were immunogold labeled using one, two or three of eight different affinity-purified antibodies to four CNS connexins (Cx26, Cx32, Cx36 and Cx47; see Table 1, antibodies used at 10 μg/ml). Goat anti-rabbit IgG and goat anti-mouse IgG conjugated to 6-nm, 12-nm and 18-nm gold beads were from Jackson ImmunoResearch, and goat anti-rabbit IgG conjugated to 30-nm gold was from BBInternational, Ltd. (Ted Pella, Inc.; Redding, CA, USA). For triple labeling, one sample of P28 rat LC was first double labeled with monoclonal antibody to Cx36 plus polyclonal antibody to Cx32, rinsed and counter labeled with goat anti-mouse 18-nm gold and goat anti-rabbit 6-nm gold. This replica was then rinsed and labeled with the third primary antibody, rabbit anti-Cx47, and counter-labeled with goat anti-rabbit 12-nm gold. Although this sequence provides unambiguous labeling for Cx32 (6-nm gold) and Cx36 (18-nm gold), a small but undetermined fraction of 12-nm gold for Cx47 may represent artifactual binding to residual unreacted bi-valent goat anti-rabbit antibody on Cx32. Nevertheless, this triple-labeling procedure provided the advantage of more efficient detection of oligodendrocyte gap junctions and confirmation of the activity of the Cx32 antibodies and relative abundance of Cx32 in those junctions. A second sample of P14 rat LC was triple labeled for Cx26+Cx32, followed by Cx47, as above.

Controls included omission of primary antibodies to each target connexin, as well as initial “blind” examination of most replicas (i.e., without knowledge of exact antibody labels or sizes of gold beads for specific connexins). The smaller gold beads label at higher efficiency than larger gold beads, in the ratio of 4:2:1:1 for 6-nm, 12-nm, 18-nm, and 30-nm gold (Rash and Yasumura, 1999;Nagy et al., 2004;Kamasawa et al., 2006). We often chose the less efficient label for Cx36 so that more efficient labels could be used to detect Cx26 or Cx32. After labeling, the replicas were air dried, a stabilizing 20-nm coat of carbon was applied to the labeled side of the replica, and the Lexan support film was removed by immersion of replicas in dichloroethane for 6−9 h, followed by air drying at 60°C.

The high specificity of immunogold labeling, in combination with the high visibility of gold beads, facilitated detection of the relatively rare neuronal and glial gap junctions in developing LC. In most samples, two sizes of gold beads were used for one or both target connexins. Because each gold bead is independently targeted, multiple examples of each of two sizes of gold for each connexin provides multiple independent confirmations of specificity of connexin labels (Kamasawa et al., 2006).

Electron Microscopy

Labeled replicas were examined at 100 kV in a JEOL 2000 EX-II TEM equipped with a ±60° tilting stage or in a JEOL 1200 EX TEM equipped with a ±45° tilting stage (JEOL, Inc., Peabody MA). Gap junctions and cells were photographed as stereoscopic pairs having an 8° included angle, and all images were analyzed stereoscopically. High-resolution digital images (20−80 MByte) were obtained from electron microscope negatives using an ArtixScan 2000f digital scanning device (Microtek, Carson, CA, USA) and processed using Photoshop 7.01 and

CS2 (Adobe Systems, San Jose, CA). Contrast range was optimized using “levels”, and where appropriate, the contrast range of displaced Lexan and carbon-coated debris was reduced by selected area “dodging” using “brightness/contrast” functions. Selected images are presented as stereoscopic pairs or as reversed stereoscopic pairs, as noted. Stereoscopic viewing, including viewing reversed stereoscopic images, was essential for discriminating 6-nm gold beads from replicated intramembrane particles (IMPs) and pits, which may be 6−10 nm and of greater electron opacity than the 6-nm gold labels (Kamasawa et al., 2006).

The primary search strategy was to search at 10,000x magnification for individual gold beads or small clusters, verify that the beads were on gap junctions, and photograph the cell without initially attempting to identify the cell type. Cells and surrounding membranes were photographed at 10,000x and areas containing gap junctions were photographed at 50,000x or 100,000x magnification. Because identities of small portions of cells in complex neuropil cannot be determined at the low magnification used for scanning replicas, this search strategy also precluded bias in assigning labeled connexins/gap junctions to neurons *vs.* glia. However, because most neuronal gap junctions were small (<100 connexons / <0.1μm in diameter), use of less-efficient 18-nm gold beads to detect Cx36 may have resulted in an underestimate of the number of Cx36-containing neuronal gap junctions (Kamasawa et al., 2006).

Estimation of areas of LC examined by FRIL: In freeze fracture and FRIL, the fracture plane primarily exposes split membrane surfaces. In complex neuropil, the fracture plane randomly samples all membranes in its path, and exposes only relatively small areas of cytoplasm or nucleoplasm (i.e., <20% of tissue surface). Each grid opening in a 200 mesh gold “index” grid has 5,000 μm^2 of examinable area. Typically, the LC neuropil overlies 6−12 grid openings (i.e.,30,000 μm^2 to 60,000 μm^2 per LC neuropil) *vs.* 1,000,000 μm^2 total open area per grid (i.e., LC occupies only about 3−6% of the total open area in each grid), and prior confocal grid mapping allowed narrowing of the searches primarily to those limited areas. For estimation of areas of plasma membrane examined (Table 2 in Results), each grid opening was divided into quadrants (ca. 1250 μm^2 per quadrant); and where necessary, each quadrant was divided into sub-quadrants (300 μm^2 per sixteenth opening). Because of membrane contour, membrane areas are actually about twice those values, but this increase would be reduced by the area of cross-fractured cytoplasm (< 20% of total area). Some quadrants were essentially obliterated by knife scrapes (or were perforated during removal of Lexan), and these were not included as "examined neuropil". Based on these considerations, our summed values for examined areas are underestimates, but they are useful for "order of magnitude" comparisons.

Identification of neurons vs. glia in freeze-fracture replicas

Neurons and glia were identified in freeze-fracture replicas based on 23 inclusive and exclusive criteria (Rash et al., 1997). In addition, leptomeningeal cells in control replicas were identified by their anatomical location at the surface of the brain or spinal cord, close proximity to collagen fibers, presence of tight junctions, and by abundant Cx26 in their gap junctions (Nagy and Dermietzel, 2000;Mercier and Hatton, 2001;Nagy et al., 2001;Nagy et al., 2004).

Criteria for identifying gap junctions in freeze-fracture replicas

Gap junctions were identified based on established criteria (Goodenough and Revel, 1970;Gilula et al., 1972;Rash et al., 1997,1998), including: a) uniform 8−9 nm diameter IMPs in their P-faces and uniform 8−9 nm diameter pits in their E-faces, both having 10-nm center-to-center spacing; b) close packing of IMPs/pits, often in regular hexagonal array; c) maintained alignment of the rows of P-face IMPs and E-face pits where the fracture plane steps from P-face to E-face within the gap junction; and d) narrowing of the extracellular space to 2−3 nm within the border of those few gap junctions in which both P- and E-faces are exposed. This report uses the internationally-recognized terminology for describing membrane faces in

freeze-fracture replicas (Branton et al., 1975), wherein replicated "***p***rotoplasmic" fracture faces are designated by the mnemonic "P-face" and the complementary "***e***xtraplasmic" leaflets (extracellular, extranuclear, extramitochondrial) are designated "E-faces".

RESULTS

Neurons in the locus coeruleus contain Cx36

Both polyclonal and monoclonal antibodies against Cx36 produced immunofluorescence labeling in the LC of rat (Fig. 1A-D) and mouse (Fig. 1E) LC. At postnatal day 7 (P7) in rat brain, a distinctly higher density of Cx36 was found in the LC compared with immediately surrounding brainstem regions, such that Cx36-positive puncta clearly delineated the cell-body-rich region of the nucleus (Fig. 1A). Immunofluorescence consisted of densely distributed Cx36-positive puncta interspersed among LC neurons (Fig. 1B). In adult rat LC, the density of labeling for Cx36 was markedly reduced compared to P7, but immunopositive puncta were still present in abundance (Fig. 1C,D). Similar labeling was observed in adult mouse LC (Fig. 1E), although the density of Cx36 puncta was somewhat lower compared with that in adult rat LC.

As in other CNS locations, labeling for Cx36 in the LC was absent in Cx36 knockout mice, as shown using monoclonal anti-Cx36 39−4200 (Fig. 1F). In both adult rats and mice, Cx36-positive puncta were concentrated within the body of the nucleus, which contains somata and dendrites of LC neurons. Cx36-puncta were present at much lower levels in regions around the nucleus ("pericoerulear"), displaying a sharp reduction in density outside the nucleus (Fig. 1A,C). Cx36-positive puncta were generally smaller in the LC of adult compared with neonatal brain, and appeared to be finer in adult LC than those that we have observed in other regions of the CNS, such as the retina, amygdala and inferior olive (Rash et al., 2000;2001b;Li et al., 2004b 2004c;Kamasawa et al., 2006). Nevertheless, Cx36 labeling was remarkable in that it clearly delineated the nucleus from adjacent structures, which were largely devoid of labeling for Cx36.

Cx36 immunofluorescent puncta in z-stack images of adult rat LC viewed as stereoscopic images (Fig. 2) were more clearly identifiable and exhibited a density that we estimate was comparable to that in the inferior olive. However, no distinct pattern of puncta was discerned. In contrast to the specific and reliable detection of Cx36 described above in developing and adult rat LC using our standard fixation protocol, perfusion of rats with a mixture of 3.75% acrolein and 2% formaldehyde produced high tissue autofluorescence and rendered Cx36 undetectable in LC as well as all other CNS regions (negative data not shown). However, Cx43 was still detectable, indicating that loss of Cx36 detection was due to reduced labeling after acrolein and not simply due to masking of its labeling by non-specific fluorescence background.

Localization of Cx26, Cx43 and Cx32 in rat LC

Immunofluorescence labeling of Cx26, Cx43 and Cx32 was examined in the LC of P7 vs. adult rats. In sections from P7 rat pups double labeled for Cx26 and Cx43, Cx26 was detected in leptomeninges but was absent in all brain parenchymal regions including the LC (Fig. 3A1), which contained instead, only faint background labeling of neuronal nuclei. Labeling for Cx43 was also present in leptomeninges, where it was co-localized with Cx26 (not shown), and was densely distributed in ependyma surrounding the fourth ventricle (Fig. 3A2). Within the LC, Cx43 was relatively sparse compared with surrounding structures (Fig. 3A2). In most brain regions at P7, immunofluorescence labeling for Cx32 was rare, and it was entirely absent in the LC as well as in regions surrounding the LC (Fig. 3B). However, clusters of Cx32 immunofluorescent puncta were found in association with a few nearby fiber tracts, as shown in the vicinity of the medial longitudinal fasciculus, where labeling was confined to a small

number of oligodendrocytes and sparsely distributed fibers, which are shown as an accompanying positive control for Cx32 detection in the nearby midline brainstem (Fig. 3C).

In sections of adult rat brain double labeled for the LC neuronal marker tyrosine hydroxylase (TH) and for each of three connexins (Fig. 3D1-G1), Cx26-puncta (Fig. 3D2) and Cx43-puncta (Fig. 3E2) were dense in both the LC and in surrounding structures. In contrast, Cx32 was more sparsely expressed in the LC than in adjacent structures (Fig. 3F2), and within the LC, was localized mainly to a few small cells having morphological features of oligodendrocytes (Fig. 3G2), including small somata with few cytoplasmic processes. Many of these small cells were seen in brainstem sections at a level immediately anterior to the LC, and double labeling for the oligodendrocyte marker CNPase and Cx32 at this level confirmed that Cx32-positive cells were oligodendrocytes (Fig. 3H1-H3). In the nucleus of the LC, higher magnification confocal images of double labeling for CNPase and Cx32 indicated that CNPase-positive cells were often surrounded by punctate labeling for Cx32 (Fig. 3I1-I3). These Cx32-positive puncta associated with oligodendrocytes are not evident at the lower magnifications due to merging of fluorescence emanating from collections of multiple puncta.

Labeling of connexins was also examined in sections from adult rat brain fixed with a mixture of 3.75% acrolein and 2% formaldehyde (Alvarez-Maucebin et al., 2000) in an attempt to determine whether this fixation protocol reveals a broader distribution and/or additional cellular locations of the connexins. With this alternative fixative, labeling for TH in the LC was robust, comparable to that observed with our standard fixative. However, immunolabeling for Cx26 and Cx32 was absent in the LC as well as most other brain regions (negative data not shown), except for very weak labeling for Cx26 observed in leptomeninges, which normally is intensely fluorescent for Cx26 following our standard fixation protocol (Rash et al., 2001a;Nagy et al., 2003b).

Distinct localization of Cx36 *vs.* Cx26 and Cx43 in adult LC

Confocal double immunolabeling studies were undertaken to determine the cellular localization relationships of Cx26, Cx36 and Cx43 in the rat LC. In sections double labeled for Cx36 and either Cx26 or Cx43, there was a clear absence of overlap between Cx36-immunopositive puncta *vs.* puncta that were either Cx26-positive (Fig. 4A1-A3) or Cx43-positive (Fig. 4B1-B3). Only on rare occasions were Cx36-puncta seen closely adjacent to Cx26- and Cx43-puncta. In contrast, double labeling of LC for Cx26 and Cx43 showed overlap of nearly all Cx26-puncta with Cx43-puncta, while only a subpopulation of the more abundant Cx43-puncta overlapped with Cx26-puncta (Fig. 4C1-C3). Sections through the LC were also double labeled for TH and Cx43 to determine the distribution of Cx43 in relation to TH-positive LC neurons. As might be expected from both the density and tight packing of these neurons in LC and the high density of astrocytic Cx43 within this nucleus, in combination with thin astrocyte sheaths surrounding each neuron (Shimizu and Imamoto, 1970;Groves and Wilson, 1980), Cx43-puncta were often seen in close proximity and surrounding these neurons (Fig. 4D1-D3). A similar distribution of Cx26 was also observed around TH-positive neurons (not shown), consistent with the substantial co-localization of Cx26 with Cx43. It should be noted, however, that Cx43 in unstained ensheathing cells examined with the limited resolution of light microscopy gives the false impression of Cx43 localized to the TH-stained neurons.

Neuronal gap junctions contain Cx36 in developing LC

We used FRIL to investigate Cx26, Cx32 and Cx36 in LC at P7, P14, P21 and P28 rats and mice. The location of LC was confirmed in replicas containing EGFP-labeled LC neurons and ependymocytes (Fig. 5A-C). Table 2 lists the numbers of replicas examined, areas of LC that were examined by raster scanning at 10,000x, ages of animals, number of neuronal and glial gap junctions found, and immunogold labels present.

In a replica from P14 rat LC that was double-labeled for Cx26+Cx36, five neuronal gap junctions (three of which are illustrated) were labeled for Cx36 (Fig. 5D-F; 12-nm gold beads), but none were labeled for Cx26 (6-nm and 18-nm gold beads, none present). Moreover, Cx26 was not detected on the few astrocyte gap junctions encountered at P14, consistent with LM immunofluorescence images from P7. (See below for evidence that the absence of Cx26 was not a "false negative" based on demonstration of the efficacy of the Cx26 antibodies).

In a replica from P14 rat that was double-labeled for Cx32+Cx36, one neuronal gap junction was found, and it was strongly labeled for Cx36 (Figs. 5G,H; 6-nm and 18-nm gold beads). Cx32 (labeled with 12-nm gold beads; none present) was not detected in neuronal gap junctions and was only very weakly detected in oligodendrocyte gap junctions (see below), which begin to appear at about this time in many other brain regions (Yamamoto et al., 1992;Nagy et al., 1999;Nagy et al., 2003b). Similarly, in P21 mouse LC labeled for Cx32+Cx36, one neuronal gap junction labeled for Cx36 was found on a small diameter dendrite (Fig. 6), but Cx32 was not detected in neuronal or astrocyte gap junctions.

Oligodendrocyte gap junctions in developing LC are rare; astrocyte gap junctions contain limited Cx26

In P14 rat LC examined by FRIL, oligodendrocyte gap junctions were extremely rare, and Cx32 was weakly detected by FRIL in only a single small oligodendrocyte gap junction (Fig. 7A) that was located within the edge of a "reciprocal patch" (Li et al., 2004a) of large IMPs on the outer surface of myelin. Likewise, in mice, Cx26 was only weakly detected in a single astrocyte/astrocyte gap junction in the LC of a P21 EGFP mouse (Fig. 7B). As one control, the same aliquot of anti-Cx26 antibodies and the same secondary antibodies were demonstrated to label gap junctions of leptomeninges ensheathing P28 cerebellum (Fig. 7C) in a sample that was prepared simultaneously with the replicas illustrated in Fig. 7A-B. (Because of limited sample area in all FRIL replicas, pia mater is not present in samples of LC, requiring analysis of leptomeninges from other CNS regions.) This strong labeling of Cx26 by both 6-nm and 18-nm gold beads in a companion "control" tissue demonstrated that the absence of Cx26 in P14 LC was not due to failure of primary or secondary antibodies. Moreover, those same secondary antibodies were used to label Cx32 in Fig. 7A, with only that one gap junction found at P14. Thus, FRIL data from P14 and P21 rat LC support immunofluorescence data suggesting absence of Cx26 in P7 rat LC in both neurons and glial cells.

Cx36 in neurons of adult LC; Cx32 only in oligodendrocytes

In a replica of adult rat LC that was triple-labeled -- first for Cx32+Cx36, followed by labeling for Cx47 (Fig. 8A-C) -- two neuronal gap junctions were found, and both were labeled for Cx36 (Fig. 8; 18-nm gold), but neither was labeled for Cx32 or Cx47 (Fig. 8C; 6-nm [none present] and 12-nm gold [one present but on the wrong side of the replica]). However,within the same replica, gold labels for both Cx32 and Cx47 were abundant in oligodendrocyte gap junctions (see next section). Even in the neuronal gap junction detected with an apparent gold bead for Cx47 nearby, stereoscopic imaging revealed that the gold bead for Cx47 was on the Lexan-coated side of the replica (Fig. 8C, arrow), and hence, was confirmed to represent non-specific "background" (Rash and Yasumura, 1999).

Although larger gap junctions are more readily detected by FRIL based on greater numbers of high visibility immunogold beads, only two small gap junctions (<50 connexons) were detected in adult LC (Fig. 8), suggesting that neuronal gap junctions are smaller and less abundant in adult LC than in early postnatal development, as suggested by LM (Fig. 1B,D). As in developing rat and mouse LC (Figs. 5,6), the small neuronal gap junctions in adult rat LC had connexons in regular hexagonal array (Fig. 8).

Neuronal coupling partners

When gap junctions were identified in neuronal E-faces (Figs. 5E,F,6,8B), the cellular coupling partners were labeled for Cx36 and not for Cx32 or Cx26, thereby documenting that in all cases where the identities of both cells could be determined based on ultrastructural criteria, neuronal coupling partners were neurons and not glial cells. Of these, all except one (Fig. 5D) were on small dendrites (Figs. 5G,8A-B), involving either another small dendrite or an axon terminal (Fig. 6A). Overall, we estimate that Cx36-containing neuronal gap junctions were present at a density of ca. 1.4 per 10,000 μm^2 of identified neuronal plasma membrane (i.e., 9 gap junctions in 66,400 μm^2 of LC membrane examined), ranging from 0.3 to 2.2 per 10,000 μm^2 at the various ages examined (Table 2).

Cx32: In gap junctions or as dispersed connexons?

At P7 and P14, myelin was poorly developed within the body of the LC, with only a few lightly myelinated axons detected. By P28 (nominally adult), however, myelinated fibers were abundant. Cx32 was found in more than 20 oligodendrocyte gap junctions, almost all of which were on three oligodendrocyte somata (Fig. 9A), with Cx32 co-localized with Cx47 in most gap junctions on oligodendrocyte somata, cytoplasmic processes, and myelin. For example, in the same triple-labeled replica as the Cx36-labeled neuronal gap junctions illustrated in Figure 8, Cx32 was abundant, but only in oligodendrocyte gap junctions (Fig. 9A-C; 6-nm gold beads). In this example, seven gap junctions (Fig. 9A, five ovals surrounding individual gap junctions and one rectangle delineating two gap junctions; enlarged as Fig. 9B) on the somatic plasma membrane of an oligodendrocyte cell body were labeled for Cx32 (Fig. 9C; 6-nm gold beads, arrowheads). Cx47, which was recently established as the second but predominant connexin in oligodendrocyte gap junctions [(Kamasawa et al., 2005); also see (Odermatt et al., 2003)], was also heavily labeled in the same gap junctions (Fig. 9A-C; 12-nm gold beads). In other oligodendrocyte gap junctions, Cx47 was detected without Cx32 (not shown), suggesting that Cx47 becomes abundant prior to Cx32, coincident with the increase in Cx43 at oligodendrocyte-to-astrocyte gap junctions (Nagy et al., 1999). As previously documented in other CNS regions (Rash et al., 2001a;Rash et al., 2001b), Cx32 was present only oligodendrocytes, in the oligodendrocyte-side of astrocyte-to-oligodendrocyte gap junctions, and never in the plasma membranes of astrocytic, neuronal or ependymocyte gap junctions. Moreover, labeling for Cx32 and Cx47 was not detectable above the otherwise very low background among dispersed IMPs, either in oligodendrocytes or at sites of neuron/astrocyte apposition. Thus, in the same replica, neuronal gap junctions were labeled for Cx36 but not for Cx32, whereas oligodendrocyte gap junctions were labeled for Cx32 and Cx47 but not for Cx36.

Despite extensive searches of 14 FRIL replicas of LC, we found no gap junctions linking neurons with any type of glial cell, regardless of age of animal or connexin examined. Equally important, in samples with very low background and high signal-to-noise ratio (Rash and Yasumura, 1999), we found no evidence for Cx26, Cx32 or Cx36 labeling of dispersed connexons (i.e., as distinctive 9-nm IMPs) within neuronal plasma membranes at any age.

DISCUSSION

Gap junctions in developing and adult LC

Neurons in the LC are extensively coupled during early postnatal development, with synchronized electrical oscillatory activity and electrical and tracer coupling demonstrated, both strongly suggestive of inter-neuronal gap junctions (Christie et al., 1989;Christie and Jelinek, 1993;Alvarez et al., 2002). The presence of neuronal gap junctions in adult LC has been more uncertain because mature LC neurons failed to exhibit detectable dye-coupling, but nevertheless displayed synchronous oscillations that were blocked by the gap junction

uncoupling agent carbenoxolone, suggesting that weak coupling of these neurons persists into adulthood (Travagli et al., 1995). This report provides immunofluorescence data documenting abundant Cx36 puncta in LC, and FRIL data documenting Cx36-containing gap junctions linking LC neurons in both postnatal and adult animals. The fewer and smaller gap junctions observed in adult compared with postnatal LC may account for the reduced neuronal coupling in adult.

Connexin composition of neuronal *vs.* glial gap junctions in LC

Extensive coupling and large numbers of gap junctions between glial cells in the CNS is well established (Brightman and Reese, 1969;Gutnick et al., 1981;Mugnaini, 1986;Kettenmann and Ransom, 1988;Butt and Ransom, 1989;Rash et al., 1997). Likewise, the existence of gap junctions/electrical synapses between mammalian neurons, albeit not their prevalence nor their connexin composition, has been reported over the past three decades (reviewed by Sotelo and Korn, 1978;Nagy and Dermietzel, 2000). Early on, it was proposed that neurons share gap junctions only with neurons, and that glia share intercellular gap junctions only with glia (Brightman and Reese, 1969;Mugnaini, 1986). This “restricted coupling partner” hypothesis gained support based on TEM and FRIL immunocytochemical data showing that neuronal, astrocytic and oligodendrocytic gap junctions each express different complements of connexins (Nagy and Rash, 2000;Nagy and Dermietzel, 2000;Rash et al., 2000, 2001b;Kamasawa et al., 2005;Fukuda et al., 2006), with Cx43, Cx30 and (in limited areas) Cx26 in astrocytes and leptomeninges (Li et al., 1997;Nagy et al., 1999,2001;Rash et al., 2001b); Cx29, Cx32 and Cx47 in oligodendrocytes (Rash et al., 2001a,2001b;Nagy et al., 2004;Kamasawa et al., 2005); and Cx36 exclusively in neurons (Rash et al., 2001b;Fukuda et al., 2006), extending data from immunofluorescence analysis and thin-section immunocytochemistry (Yamamoto et al., 1990a,1990b;Scherer et al., 1995;Mercier and Hatton, 2001;Altevogt et al., 2002;Kleopas et al., 2004;Rash et al., 2005).

However, based on *in situ* hybridization and RT-PCR detection of mRNAs for Cx26, Cx32 and Cx43 in neurons (Micevych and Abelson, 1991;Micevych et al., 1996;Venance et al., 2000;Zhang et al., 2000), an alternative “shared-connexins/mixed-coupling” hypothesis arose and seemingly was supported by reports of electrical and dye coupling of neurons with glia (Nedergaard, 1994;Alvarez-Maubecin et al., 2000;Van Bockstaele et al., 2004) and by reported immunocytochemical labeling for “glial” Cx26, Cx32 and Cx43 in neurons (Nadarajah et al., 1997;Kelsell et al., 1997;Nadarajah and Parnavelas, 1999;Alvarez-Maubecin et al., 2000;Zhang et al., 2000;Bittman et al., 2002). Thus, the report by Alvarez-Maubecin (2000) of abundant Cx26 and Cx32 labeling of putative gap junctions in LC neurons during early postnatal development, and their subsequent report of biochemical detection of Cx32 (but inability to detect Cx26) in developing LC (Van Bockstaele et al., 2004) were particularly intriguing, potentially suggesting novel expression patterns of connexins and novel gap junctional communication properties of these neurons. Instead, of the five connexins tested, current results revealed that gap junctions between LC neurons contain exclusively Cx36, whereas Cx26 and Cx32 are essentially not present in LC at P7 and P14, and by P28, are present in and restricted exclusively to astrocyte and oligodendrocyte gap junctions, respectively.

How abundant are neuronal gap junctions in LC, and do they contain Cx32 or Cx26?

The basis for the discrepancies between current findings and those of others was examined in greater detail. First, Alvarez-Maubecin et al. (2000) reported that Cx26 and Cx32 were abundantly localized by thin-section immunoEM to areas of apposed plasma membrane that “tended to approach”, which they proposed to represent gap junctions. However, none of the areas with closely associated silver/gold beads were shown to meet the classical criteria for designation as gap junctions, namely heptalaminar parallel arrangement of contacting plasma membranes (Brightman and Reese, 1969;Sotelo and Korn, 1978;Rash et al. 1998). Second, in

three thin sections from each of three animals (nine total sections), they showed silver grains, ostensibly for Cx32, on 203 putative gap junctions, involving 51% of sectioned dendrite profiles, including 19% as dendro-dendritic contacts and 32% as neuronal/glial contacts (mostly neuron/astrocyte contacts). By calculation based on nominal 0.1 μm section thickness and average dendrite profile circumference of 3−10 μm (10 μm × 0.1 μm thickness × 51%),this corresponds to an average density of 1.5−5 gap junctions per μm^2 of dendrite surface. They also reported similar high levels of Cx26/silver beads at putative neuronal/neuronal and neuronal/glial gap junctions. Those calculated densities for neuronal gap junctions would be 1,000−10,000 times greater than found in any other CNS region except retina, where gap junctions are still at least 100 times less abundant (Kamasawa et al., 2006) than described in LC (Alvarez-Maubecin et al., 2000). Based on the greater membrane sampling capability of freeze fracture, this calculated density should have allowed detection of hundreds of gap junctions in each FRIL replica of LC and dozens of gap junctions within a typical freeze-fractured dendrite surface. Instead, we found far fewer neuronal gap junctions numbers (ca. 1/6,000 μm^2; or ca. 0−4 per replica), which is similar to densities found in spinal cord, inferior olive, and suprachiasmatic nucleus (Rash et al., 1996,2000,2001b;Nagy et al., 2004; and Rash, Nagy and Dudek, unpublished observations). Third, in contrast to purported abundance Cx32 in astrocytes (Alvarez-Maubecin et al., 2000), Cx32 was not found by FRIL in astrocytes at any age, paralleling observations in all other brain regions (Dermietzel et al., 1989;Nelles et al., 1996;Kunzelmann et al., 1997;Dermietzel, 1998;Rash et al., 2001b;Nagy et al., 2003b;Kamasawa et al., 2005). Fourth, consistent with our reports that detection of Cx26 and Cx32 is particularly sensitive to tissue fixation conditions (Li et al., 1997;Nagy et al., 2001, 2003a,b), we found that the stronger 3.75% acrolein/2% formaldehyde fixative of Alvarez-Maubecin (2000) applied under our conditions of immunohistochemistry abolished all labeling of Cx32 and Cx26 in brain parenchyma and greatly reduced Cx26 labeling in leptomeninges. These data suggest that the reported detection of hyper-abundant Cx32 in neuronal and astrocyte plasma membranes may have resulted from creation of extraneous silver product, possibly due to overdevelopment of the silver intensification reaction in the absence of positive controls to calibrate time of silver development. [For rationale, see (Stierhof et al., 1991)].

Gap junctions not detected between neurons and astrocytes in LC

Propagation of calcium waves between neurons and glia led to proposals of neuron-to-glial coupling (Nedergaard, 1994). Subsequently, based on immunocytochemical labeling and dye-coupling data, several groups proposed the existence and abundance of neuron-to-glial gap junctions involving Cx32 and Cx26 (Nadarajah et al., 1997;Nadarajah and Parnavelas, 1999;Alvarez-Maubecin et al., 2000;Colwell, 2000;Bittman et al., 2002). However, based on FRIL analysis, we found no evidence for gap junctions linking neurons to astrocytes in the LC. Where both cells could be identified at neuronal gap junctions, both coupling partners were identified as neurons. Moreover, all neuronal gap junctions detected by FRIL contained Cx36 but none contained Cx32 or Cx26. In addition, the restricted localization of Cx36 to neuronal gap junctions, together with the absence of immunofluorescence overlap between Cx36 and either Cx26 or Cx43, further indicate the lack of heterologous coupling between Cx36 and astrocytic Cx26 or Cx43. Based on our previous detection of gap junctions with as few as two connexons labeled for Cx32 (Meier et al., 2004), we also conclude that neither Cx32 nor Cx26 occur in neuronal plasma membranes as abundant but dispersed connexons (i.e., not detectably above the very low “background”).

Possible sources of observed dye coupling of astrocytes to neurons

Neuronal somata in the adult LC are ensheathed by one or more thin glial processes (Shimizu and Imamoto, 1970;Groves and Wilson, 1980), just as in other brain regions, where thin-section immunoEM revealed labeling for Cx43 on gap junctions between astrocyte processes but not between astrocytes and neurons (Yamamoto, et al., 1990a,1990b,1992;Nagy et al., 2004). By

immunofluorescence, these Cx43-positive puncta often surround neurons, giving the appearance of Cx43 puncta on neuronal somata, as observed in the present study. Likewise, given the rich ensheathment of LC neurons by astrocytes, injection of dye into single astrocytes or neurons in slice preparations may have resulted in concurrent penetration through surrounding astrocyte sheaths into neurons, providing a potential pathway to account for the observed dye transfer between astrocytes and neurons (Alvarez-Maubecin et al., 2000). Alternatively, cytoplasmic fusion of damaged neurons with astrocyte processes may have occurred at the cut surfaces of tissues slices, with resultant artifactual heterologous intercellular dye transfer (Bennett and Zukin, 2004).

Functional implications of LC neuronal coupling and gap junctions composed of Cx36

The LC-noradrenergic system, via its widespread and dense innervation of many brain areas, is thought to contribute to cognitive performance and related functions such as learning, memory, and attention (Marien et al., 2004;Aston-Jones and Cohen, 2005,2006). It has been noted that electrical coupling between activated LC neurons would result in the synchronized release of norepinephrine in most, if not all, projection areas of the LC (Christie et al., 1989;Travagli et al., 1995;Ishimatsu and Williams, 1996). Coordinated release of norepinephrine at many LC target sites would be consistent with the presumed ability for the LC to simultaneously influence broad areas of brain in the behavioral functions of this nucleus. The effects of norepinephrine may be even more far reaching in view of reports that it has a modulatory action on gap junctional coupling between networks of cortical neurons (Rörig et al., 1995;Roerig and Feller, 2000). Electrical synapses in neural networks were proposed to mediate synchronous activity and fast oscillations (i.e., gamma 30−80 Hz and high-frequency 200−500 Hz activities) among ensembles of neurons (Bennett and Zukin, 2004;Christie et al., 2005), which are thought to contribute to such cognitive processes as perception, attention and consciousness (Singer and Gray, 1995;Singer et al., 1999;Diesmann et al., 1999). Thus, in adults, oscillatory synchronization *via* weak gap junctional coupling at small gap junctions between LC neurons, together with norepinephrine actions on coupling in LC projection areas may contribute to the widespread influence of LC activity on behavioral state. In view of these considerations, deficits in LC neuronal gap junctional coupling may underlie some of the observed behavioral and neurological impairments in Cx36 KO mice (Hormuzdi et al., 2001;Frisch et al., 2005). Based on similar reasoning, the report of Cx32 and Cx26 localization in LC neurons might have suggested neurological impairments in human subjects with genetic abnormalities involving Cx26 and Cx32, whose clinical manifestations included sensorineural hearing loss (Kelsell et al., 1997) and peripheral neuropathy, respectively (Bergoffen et al., 1993;Bahr et al., 1999). Our results, however, indicate that studies designed to detect such potentially LC-based neuronal impairments in humans with mutations in Cx32 and Cx26 would be unwarranted.

Acknowledgements:

Supported by NIH grants NS-44010, NS-44395 (JER) and the CIHR (JIN). We thank David Paul for providing Cx36 knockout mouse breeding pairs, and Brett Mclean for excellent technical assistance.

Glossary

Cx, connexin; EF, extraplasmic face or E-face; EGFP, enhanced green fluorescent protein; FRIL, freeze-fracture replica immunogold labeling; IMP, intramembrane particle; LC, locus coeruleus; LE, labeling efficiency; LM, light microscopy; PF, protoplasmic face or P-face PSD, postsynaptic density; SDS, sodium dodecylsulfate detergent; TBS, Tris-buffered saline; TBSTr, Tris-buffered saline plus 0.3% Triton X-100; TEM, transmission electron microscopy; TH, tyrosine hydroxylase.

Reference List

Altevogt BM, Kleopas KA, Postma FR, Scherer SS, Paul D. Connexin29 is uniquely distributed within myelinating glial cells of the central and peripheral nervous systems. J Neurosci 2002;22:6458–6470. [PubMed: 12151525]

Altevogt BM, Paul DL. Four classes of intercellular channels between glial cells in the CNS. J Neurosci 2004;24:4313–4323. [PubMed: 15128845]

Alvarez VA, Chow CC, Van Bockstaele EJ, Williams JT. Frequency-dependent synchrony in locus ceruleus: Role of electrotonic coupling. Proc Natl Acad Sci (USA) 2002;99:4032–4036. [PubMed: 11904447]

Alvarez-Maubecin V, García-Hernández F, Williams JT, Van Bockstaele EJ. Functional coupling between neurons and glia. J Neurosci 2000;20:4091–4098. [PubMed: 10818144]

Andrzejewski M, Muckenhoff K, Scheid P, Ballantyne D. Synchronized rhythms in chemosensitive neurons of the locus coeruleus in the absence of chemical synaptic transmission. Resp Physiol 2001;129:123–140.

Aston-Jones G, Cohen JD. An integrative theory of locus coeruleus-norepinephrine function: Adaptive gain and optimal performance. Ann Rev Neurosci 2005;28:403–450. [PubMed: 16022602]

Aston-Jones G, Cohen JD. Adaptive gain and the role of the locus coeruleus-norepinephrine system in optimal performance. J Comp Neurol 2006;493:99–110. [PubMed: 16254995]

Bahr M, Andres F, Timmerman V, Nelis ME, Van Broeckhoven C, Dichgans J. Central visual, acoustic, and motor pathway involvement in a Charcot-Marie-Tooth family with an Asn205Ser mutation in the connexin 32 gene. J Neurol Neurosurg Psychiatry 1999;66:202–206. [PubMed: 10071100]

Ballantyne D, Andrzejewski M, Muckenhoff K, Scheid P. Rhythms, synchrony and electrical coupling in the Locus coeruleus. Resp Physiol Neurobiol 2004;143:199–214.

Bennett MVL, Zukin RS. Electrical coupling and neuronal synchronization in the mammalian brain. Neuron 2004;41:495–511. [PubMed: 14980200]

Bergoffen J, Scherer SS, Wang S, Oronzi-Scott M, Paul D, Chen K, Lensch MW, Chance P, Fischbeck K. Connexin mutations in X-linked Charcot-Marie-Tooth disease. Science 1993;262:2039–2042. [PubMed: 8266101]

Bittman K, Becker DL, Circarata F, Parnavelas JG. Connexin expression in homotypic and heterotypic cell coupling in the developing cerebral cortex. J Comp Neurol 2002;443:201–212. [PubMed: 11807831]

Branton D, Bullivant S, Gilula NB, Karnovsky MJ, Moor H, Northcote DH, Packer L, Satir B, Satir P, Speth V, Staehelin LA, Steere RL, Weinstein RS. Freeze-etching nomenclature. Science 1975;190:54–56. [PubMed: 1166299]

Brightman MW, Reese TS. Junctions between intimately apposed cell membranes in the vertebrate brain. J Cell Biol 1969;40:648–677. [PubMed: 5765759]

Bruzzone R, Dermietzel R. Structure and function of gap junctions in the developing brain. Cell Tissue Res 2006;326:239–248. [PubMed: 16896946]

Butt AM, Ransom BR. Visualization of oligodendrocytes and astrocytes in the intact rat optic nerve by intracellular injection of Lucifer Yellow and horseradish peroxidase. Glia 1989;2:470–475. [PubMed: 2531727]

Charles AC. Glia-neuron intercellular calcium signalling. Dev Neurosci 1994;16:196–206. [PubMed: 7705224]

Charles AC, Kodali SK, Tyndale RF. Intercellular calcium waves in neurons. Mol Cell Neurosci 1996;7:337–353. [PubMed: 8812061]

Christie JM, Bark C, Hormuzdi SG, Helbig I, Monyer H, Westbrook GL. Connexin36 mediates spike synchrony in olfactory bulb glomeruli. Neuron 2005;46:761–772. [PubMed: 15924862]

Christie JM, Jelinek HF. Dye-coupling among neurons of the rat locus coeruleus during postnatal development. Neuroscience 1993;56:129–137. [PubMed: 7694183]

Christie MJ, Williams JT, North RA. Electrical coupling synchronizes subthreshold activity in locus coeruleus neurons *in vitro* from neonatal rats. J Neurosci 1989;9:3584–3589. [PubMed: 2795142]

Colwell CS. Rhythmic coupling among cells in the suprachiasmatic nucleus. J Neurobiol 2000;43:379–388. [PubMed: 10861563]

Condorelli DF, Belluardo N, Trovato-Salinaro A, Mudo G. Expression of Cx36 in mammalian neurons. Brain Res Brain Res Rev 2000;32:72–85. [PubMed: 10751658]

Condorelli DF, Parenti R, Spinella F, Salinaro AT, Belluardo N, Cardile V, Cicirata F. Cloning of a new gap junction gene (Cx36) highly expressed in mammalian brain neurons. Eur J Neurosci 1998;10:1202–1208. [PubMed: 9753189]

Dermietzel R. Diversification of gap junction proteins (connexins) in the central nervous system and the concept of functional compartments. Cell Biol Internat 1998;22:719–730.

Dermietzel R, Traub O, Hwang TK, Beyer E, Bennett MVL, Spray DC, Willecke K. Differential expression of three gap junction proteins in developing and mature brain tissues. Proc Natl Acad Sci (USA) 1989;86:10148–10152. [PubMed: 2557621]

Diesmann M, Gewaltig MO, Aertsen A. Stable propagation of synchronous spiking in cortical neural networks. Nature 1999;402:529–533. [PubMed: 10591212]

Dinchuk JE, Johnson TJA, Rash JE. Postreplication labeling of E-leaflet molecules: Membrane immunoglobulins localized in sectioned labeled replicas examined by TEM and HVEM. J Electron Microsc Tech 1987;7:1–16. [PubMed: 2464678]

Frisch C, De Souza-Silva MA, Sohl G, Güldenagel M, Willecke K, Huston JP, Dere E. Stimulus complexity dependent memory impairment and changes in motor performance after deletion of the neuronal gap junction protein connexin36 in mice. Behav Brain Res 2005;157:177–185. [PubMed: 15617784]

Fujimoto K. Freeze-fracture replica electron microscopy combined with SDS digestion for cytochemical labeling of integral membrane proteins. Application to the immunogold labeling of intercellular junctional complexes. J Cell Sci 1995;108:3443–3449. [PubMed: 8586656]

Fukuda T, Kosaka T, Singer W, Galuske RAW. Gap junctions among dendrites of cortical GABAergic neurons establish a dense and widespread intercolumnar network. J Neurosci 2006;26:3434–3443. [PubMed: 16571750]

Fulton BP. Gap junctions in the developing nervous system. Persp Dev Neurobio 1995;2:327–334.

Gilula NB, Reeves OR, Steinbach A. Metabolic coupling, ionic coupling and cell contacts. Nature 1972;235:262–265. [PubMed: 4551177]

Goodenough DA, Revel JP. A fine structural analysis of intercellular junctions in the mouse liver. J Cell Biol 1970;45:272–290. [PubMed: 4105112]

Groves PM, Wilson CJ. Fine structure of rat locus coeruleus. J Comp Neurol 1980;193:841–852. [PubMed: 7430440]

Gutnick MJ, Connors BW, Ransom BR. Dye-coupling between glial cells in the guinea pig neocortical slice. Brain Research 1981;213:486–492. [PubMed: 7248773]

Hassinger TD, Atkinson PB, Strecker GJ, Whalen LR, Dudek FE, Kossell AH, Kater SB. Evidence for glutamate-mediated activation of hippocampal neurons by glial calcium waves. J Neurobiology 1995;28:159–170.

Hormuzdi SG, Filippov MA, Mitropoulou G, Monyer H, Bruzzone R. Electrical synapses: a dynamic signaling system that shapes the activity of neuronal networks. Biochim Biophys Acta (BBA) - Biomembranes 2004;1662:113–137.

Hormuzdi SJ, Pais I, LeBeau FEN, Towers SK, Rozov A, Buhl EH, Whittington MA, Monyer H. Impaired electrical signaling disrupts gamma frequency oscillations in connexin 36-deficient mice. Neuron 2001;31:487–495. [PubMed: 11516404]

Ishimatsu M, Williams JT. Synchronous activity in locus coeruleus results from dendritic interactions in pericoerulear regions. J Neurosci 1996;16:5196–5204. [PubMed: 8756448]

Kamasawa N, Furman CS, Davidson KGV, Sampson JA, Magnie AR, Gebhardt B, Kamasawa M, Morita M, Yasumura T, Pieper M, Zumbrunnen JR, Pickard GE, Nagy JI, Rash JE. Abundance and ultrastructural diversity of neuronal gap junctions in the OFF and ON sublaminae of the inner plexiform layer of rat and mouse retina. Neuroscience 2006;142:1093–1117. [PubMed: 17010526]

Kamasawa N, Sik A, Morita M, Yasumura T, Davidson KGV, Nagy JI, Rash JE. Connexin47 and connexin32 in gap junctions of oligodendrocyte somata, myelin sheaths, paranodal loops, and Schmidt-Lanterman incisures: Implications for ionic homeostasis and potassium siphoning. Neuroscience 2005;136:65–86. [PubMed: 16203097]

Kelsell DP, Dunlop J, Stevens HP, Lench NJ, Liang JN, Parry G, Mueller MF, Leigh IM. Connexin 26 mutations in hereditary non-sydromic sensorineural deafness. Nature 1997;387:80–83. [PubMed: 9139825]

Kettenmann H, Ransom BR. Electrical coupling between astrocytes and between oligodendrocytes studied in mammalian cell cultures. Glia 1988;1:64–73. [PubMed: 2853139]

Kleopas KA, Orthmann JL, Enriquez A, Paul DL, Scherer SS. Unique distributions of the gap junction proteins connexin29, connexin32, and connexin47 in oligodendrocytes. Glia 2004;47:346–357. [PubMed: 15293232]

Kosaka T. Gap junctions between non-pyramidal cell dendrites in the rat hippocampus (CA1 and CA3 regions): a combined golgi-electron microscopy study. J Comp Neurol 1985;231:150–161. [PubMed: 3968232]

Kosaka T, Kosaka K. Intraglomerular dendritic link connected by gap junctions and chemical synapses in the mouse main olfactory bulb: Electron microscopic serial section analyses. Neuroscience 2005;131:611–625. [PubMed: 15730867]

Kunzelmann P, Blumcke I, Traub O, Dermietzel R, Willecke K. Coexpression of connexin45 and −32 in oligodendrocytes of rat brain. J Neurocytol 1997;26:17–22. [PubMed: 9154525]

Li J, Hertzberg EL, Nagy JI. Connexin32 in oligodendrocytes and association with myelinated fibers in mouse and rat brain. J Comp Neurol 1997;379:571–591. [PubMed: 9067844]

Li X, Ionescu A-V, Lynn BD, Lu S, Kamasawa N, Morita M, Davidson KGV, Yasumura T, Rash JE, Nagy JI. Connexin47, connexin29 and connexin32 co-expression in oligodendrocytes and Cx47 association with zonula occludens-1 (ZO-1) in mouse brain. Neuroscience 2004a;126:611–630. [PubMed: 15183511]

Li X, Olson C, Lu S, Kamasawa N, Yasumura T, Rash JE, Nagy JI. Neuronal connexin36 association with zonula occludens-1 protein (ZO-1) in mouse brain and interaction with the first PDZ domain of ZO-1. Eur J Neurosci 2004b;19:2132–2146. [PubMed: 15090040]

Li X, Olson C, Lu S, Nagy JI. Association of connexin36 with zonula occludens-1 in HeLa cells, βTC-3 cells, pancreas, and adrenal gland. Histochem Cell Biol 2004c;122:485–498. [PubMed: 15558297]

Marien MR, Colpaert FC, Rosenquist AC. Noradrenergic mechanisms in neurodegenerative diseases: a theory. Brain Res Brain Res Rev 2004;45:38–78. [PubMed: 15063099]

Meier C, Dermietzel R, Davidson KGV, Yasumura T, Rash JE. Connexin32-containing gap junctions in Schwann cells at the internodal zone of partial myelin compaction and in Schmidt-Lanterman incisures. J Neurosci 2004;24:3186–3198. [PubMed: 15056698]

Mercier F, Hatton GI. Connexin 26 and basic fibroblast growth factor are expressed primarily in the subpial and subependymal layers in adult brain parenchyma: Roles in stem cell proliferation and morphological plasticity? J Comp Neurol 2001;431:88–104. [PubMed: 11169992]

Micevych PE, Abelson L. Distribution of mRNAs coding for liver and heart gap junction proteins in the rat central nervous system. J Comp Neurol 1991;305:96–118. [PubMed: 1851768]

Micevych PE, Popper P, Hatton GI. Connexin 32 mRNA levels in the rat supraoptic nucleus; up-regulation prior to parturition and during lactation. Neuroendocrinology 1996;63:39–45. [PubMed: 8839353]

Montoro RJ, Yuste R. Gap junctions in developing neocortex: a review. Brain Res Rev 2004;47:216–226. [PubMed: 15572173]

Mugnaini, E. Cell junctions of astrocytes, ependyma, and related cells in the mammalian central nervous system, with emphasis on the hypothesis of a generalized functional syncytium of supporting cells. In: Fedoroff, S.; Vernadakis, A., editors. Astrocytes. I. Academic Press; New York: 1986. p. 329-371.

Nadarajah B, Jones AM, Evans WH, Parnavelas JG. Differential expression of connexins during neocortical development and neuronal circuit formation. J Neurosci 1997;17:3096–3111. [PubMed: 9096144]

Nadarajah B, Parnavelas JG. Gap junction-mediated communication in the developing and adult cerebral cortex. Novartis Found Symp 219: Gap junction-mediated intercellular coupling in health and disease 1999;219:157–170.

Nagy, JI.; Dermietzel, R. Gap junctions and connexins in the mammalian central nervous system. In: Hertzberg, EL., editor. Advances in Molecular and Cell Biology. 30. JAI Press; Greenwich: 2000. p. 323-396.

Nagy JI, Dudek FE, Rash JE. Update on connexins and gap junctions in neurons and glia in the mammalian central nervous system. Brain Res Brain Res Rev 2004;47:191–215. [PubMed: 15572172]

Nagy JI, Ionescu A-V, Lynn BD, Rash JE. Connexin29 and connexin32 at oligodendrocyte and astrocyte gap junctions and in myelin of the mouse central nervous system. J Comp Neurol 2003a;464:356–370. [PubMed: 12900929]

Nagy JI, Ionescu A-V, Lynn BD, Rash JE. Coupling of astrocyte connexins Cx26, Cx30, Cx43 to oligodendrocyte Cx29, Cx32, Cx47: Implications from normal and connexin32 knockout mice. Glia 2003b;44:205–218. [PubMed: 14603462]

Nagy JI, Li X, Rempel J, Stelmack GL, Patel D, Staines WA, Yasumura T, Rash JE. Connexin26 in adult rodent CNS: Demonstration at astrocytic gap junctions and co-localization with connexin30 and connexin43. J Comp Neurol 2001;441:302–323. [PubMed: 11745652]

Nagy JI, Patel D, Ochalski PAY, Stelmack GL. Connexin30 in rodent, cat and human brain: Selective expression in gray matter astrocytes, co-localization with connexin43 at gap junctions and late developmental appearance. Neuroscience 1999;88:447–468. [PubMed: 10197766]

Nagy JI, Rash JE. Connexins and gap junctions of astrocytes and oligodendrocytes in the CNS. Brain Res Rev 2000;32:29–44. [PubMed: 10751655]

Nedergaard M. Direct signaling from astrocytes to neurons in cultures of mammalian brain cells. Science 1994;263:1768–1771. [PubMed: 8134839]

Nelles E, Butzler C, Jung D, Temme A, Gabriel HD, Dahl U, Traub O, Stumpel F, Jungermann K, Zielasek J, Toyka KV, Dermietzel R, Willecke K. Defective propagation of signals generated by sympathetic nerve stimulation in the liver of connexin32-deficient mice. Pro Natl Acad Sci 1996;93:9565–9570.

Odermatt B, Wellershaus K, Wallraff A, Seifert G, Degen J, Euwens C, Fuss B, Bussow H, Schilling K, Steinhauser C, Willecke K. Connexin 47 (Cx47)-deficient mice with Enhanced Green Fluorescent Protein reporter gene reveal predominant oligodendrocytic expression of Cx47 and display vacuolized myelin in the CNS. J Neurosci 2003;23:4549–4559. [PubMed: 12805295]

Oyamada Y, Andrzejewski M, Muckenhoff K, Scheid P, Ballantyne D. Locus coeruleus neurones in vitro: pH-sensitive oscillations of membrane potential in an electrically coupled network. Resp Physiol 1999;118:131–147.

Parpura V, Basarky TA, Liu F, Jeftinija K, Jeftenija S, Haydon PG. Glutamate-mediated astrocyte-neuron signalling. Nature 1994;369:744–747. [PubMed: 7911978]

Paxinos, G.; Watson, C. The rat brain in stereotaxic coordinates (CD version). Academic Press; San Diego: 1998.

Peinado A, Yuste R, Katz LC. Gap junctional communication and the development of local circuits in neocortex. Cereb Cortex 1993;3:488–498. [PubMed: 8260815]

Rash JE, Davidson KGV, Kamasawa N, Yasumura T, Kamasawa M, Zhang C, Michaels R, Restrepo D, Ottersen OP, Olson C, Nagy JI. Ultrastructural localization of connexins (Cx36, Cx43, Cx45), glutamate receptors and aquaporin-4 in rodent olfactory mucosa, olfactory nerve and olfactory bulb. J Neurocytol 2005;34:307–341. [PubMed: 16841170]

Rash JE, Dillman RK, Bilhartz BL, Duffy HS, Whalen LR, Yasumura T. Mixed synapses discovered and mapped throughout mammalian spinal cord. Proc Natl Acad Sci (USA) 1996;93:4235–4239. [PubMed: 8633047]

Rash, JE.; Dillman, RK.; Morita, M.; Whalen, LR.; Guthrie, PB.; Fay-Guthrie, D.; Wheeler, DW. Grid-mapped freeze fracture: Correlative confocal laser scanning microscopy and freeze-fracture electron microscopy of preselected cells in tissue slices. In: Severs, NJ.; Shotton, DM., editors. Rapid Freezing, Freeze Fracture, and Deep Etching. Wiley-Liss, Inc.; New York, NY: 1995. p. 127-150.

Rash JE, Duffy HS, Dudek FE, Bilhartz BL, Whalen LR, Yasumura T. Grid-mapped freeze-fracture analysis of gap junctions in gray and white matter of adult rat central nervous system, with evidence for a “panglial syncytium” that is not coupled to neurons. J Comp Neurol 1997;388:265–292. [PubMed: 9368841]

Rash, JE.; Johnson, TJA.; Dinchuk, JE.; Duch, DS.; Levinson, SR. Labeling intramembrane particles in freeze-fracture replicas. In: Hui, SW., editor. Freeze-Fracture Studies of Membranes. CRC Press; Boca Raton: 1989. p. 41-59.

Rash JE, Olson CO, Pouliot WA, Davidson KGV, Yasumura T, Furman CS, Royer S, Kamasawa N, Nagy JI, Dudek FE. Connexin36, miniature neuronal gap junctions, and limited electrotonic coupling in rodent suprachiasmatic nucleus (SCN). Neuroscience. 2007in revision

Rash JE, Staines WA, Yasumura T, Patel D, Hudson CS, Stelmack GL, Nagy JI. Immunogold evidence that neuronal gap junctions in adult rat brain and spinal cord contain connexin36 (Cx36) but not Cx32 or Cx43. Proc Natl Acad Sci (USA) 2000;97:7573–7578. [PubMed: 10861019]

Rash JE, Yasumura T. Improved structural detail in freeze-fracture replicas: High-angle shadowing of gap junctions cooled below −170° C and protected by liquid nitrogen-cooled shrouds. J Electron Microsc Tech 1992;20:187–204.

Rash JE, Yasumura T. Direct immunogold labeling of connexins and aquaporin4 in freeze-fracture replicas of liver, brain and spinal cord: factors limiting quantitative analysis. Cell Tissue Res 1999;296:307–321. [PubMed: 10382274]

Rash JE, Yasumura T, Davidson K, Furman CS, Dudek FE, Nagy JI. Identification of cells expressing Cx43, Cx30, Cx26, Cx32 and Cx36 in gap junctions of rat brain and spinal cord. Cell Commun Adhes 2001a;8:315–320. [PubMed: 12064610]

Rash JE, Yasumura T, Dudek FE. Ultrastructure, histological distribution, and freeze-fracture immunocytochemistry of gap junctions in rat brain and spinal cord. Cell Biol Internat 1998;22:731–749.

Rash JE, Yasumura T, Dudek FE, Nagy JI. Cell-specific expression of connexins, and evidence for restricted gap junctional coupling between glial cells and between neurons. J Neurosci 2001b; 21:1983–2001. [PubMed: 11245683]

Roerig B, Feller MB. Neurotransmitters and gap junctions in developing neural circuits. Brain Res Brain Res Rev 2000;32:86–114. [PubMed: 10751659]

Rörig B, Klausa B, Sutor B. Beta-adrenoreceptor activation reduces dye-coupling between immature rat neocortical neurones. Neuroreport 1995;6:1811–1815. [PubMed: 8541488]

Scherer SS, Deschenes SM, Xu Y-T, Grinspan JP, Fischbeck KH, Paul DL. Connexin32 is a myelin-related protein in the PNS and CNS. J Neurosci 1995;15:8281. [PubMed: 8613761]

Scherer SS, Braun PE, Grinspan J, Collarini E, Wang D, Kamholz J. Differential regulation of the 2',3'-cyclic nucleotide 3'-phosphodiesterase gene during oligodendrocyte development. Neuron 1994;12:1363–1375. [PubMed: 8011341]

Shimizu N, Imamoto K. Fine structure of the locus coeruleus in the rat. Arch Histo Jpn 1970;31:229–246.

Singer W, Gray CM. Visual feature integration and the temporal correlation hypothesis. Ann Rev Neurosci 1995;18:555–586. [PubMed: 7605074]

Singer W, Zhang L, Velazquez JL, Carlen PL. Neuronal synchrony: a versatile code for the definition of relations? Neuron 1999;24:49–65. [PubMed: 10677026]

Sotelo C, Korn H. Morphological correlates of electrical and other interactions through low-resistance pathways between neurons of the vertebrate central nervous system. Internat Rev Cytol 1978;55:67–107.

Stierhof Y-D, Humbel BM, Schwarz H. Suitability of different silver enhancement methods applied to 1 nm colloidal gold particles: An immunoelectron microscopic study. J Electron Microsc Tech 1991;17:336–343. [PubMed: 1646315]

Travagli RA, Dunwiddie TV, Williams JT. Opioid inhibition in locus coeruleus. J Neurophysiol 1995;74:518–528. [PubMed: 7472359]

Van Bockstaele EJ, Garcia-Hernandez F, Fox K, Alvarez VA, Williams JT. Expression of connexins during development and following manipulation of afferent input in the rat locus coeruleus. Neurochem Internat 2004;45:421–428.

van den Pol AN, Ghosh PK, Liu Rj, Li Y, Aghajanian GK, Gao XB. Hypocretin (orexin) enhances neuron activity and cell synchrony in developing mouse GFP-expressing locus coeruleus. J Physiol 2002;541:169–185. [PubMed: 12015428]

Venance L, Rosov A, Blatow M, Burnashev N, Feldmeyer D, Monyer H. Connexin expression in electrically coupled postnatal rat brain neurons. Proc Natl Acad Sci (USA) 2000;97:10260–10265. [PubMed: 10944183]

Yamamoto T, Ochalski A, Hertzberg EL, Nagy JI. LM and EM immunolocalization of the gap junctional protein connexin 43 in rat brain. Brain Res 1990a;508:313–319. [PubMed: 2155040]

Yamamoto T, Ochalski A, Hertzberg EL, Nagy JI. On the organization of astrocytic gap junctions in the brain as suggested by LM and EM immunocytochemistry of connexin43 expression. J Comp Neurol 1990b;302:853–883. [PubMed: 1964467]

Yamamoto T, Vukelic J, Hertzberg EL, Nagy JI. Differential anatomical and cellular patterns of connexin43 expression during postnatal development of rat brain. Dev Brain Res 1992;66:165–180. [PubMed: 1318799]

Zhang C, Finger TE, Restrepo D. Mature olfactory receptor neurons express connexin 43. J Comp Neurol 2000;426:1–12. [PubMed: 10980480]

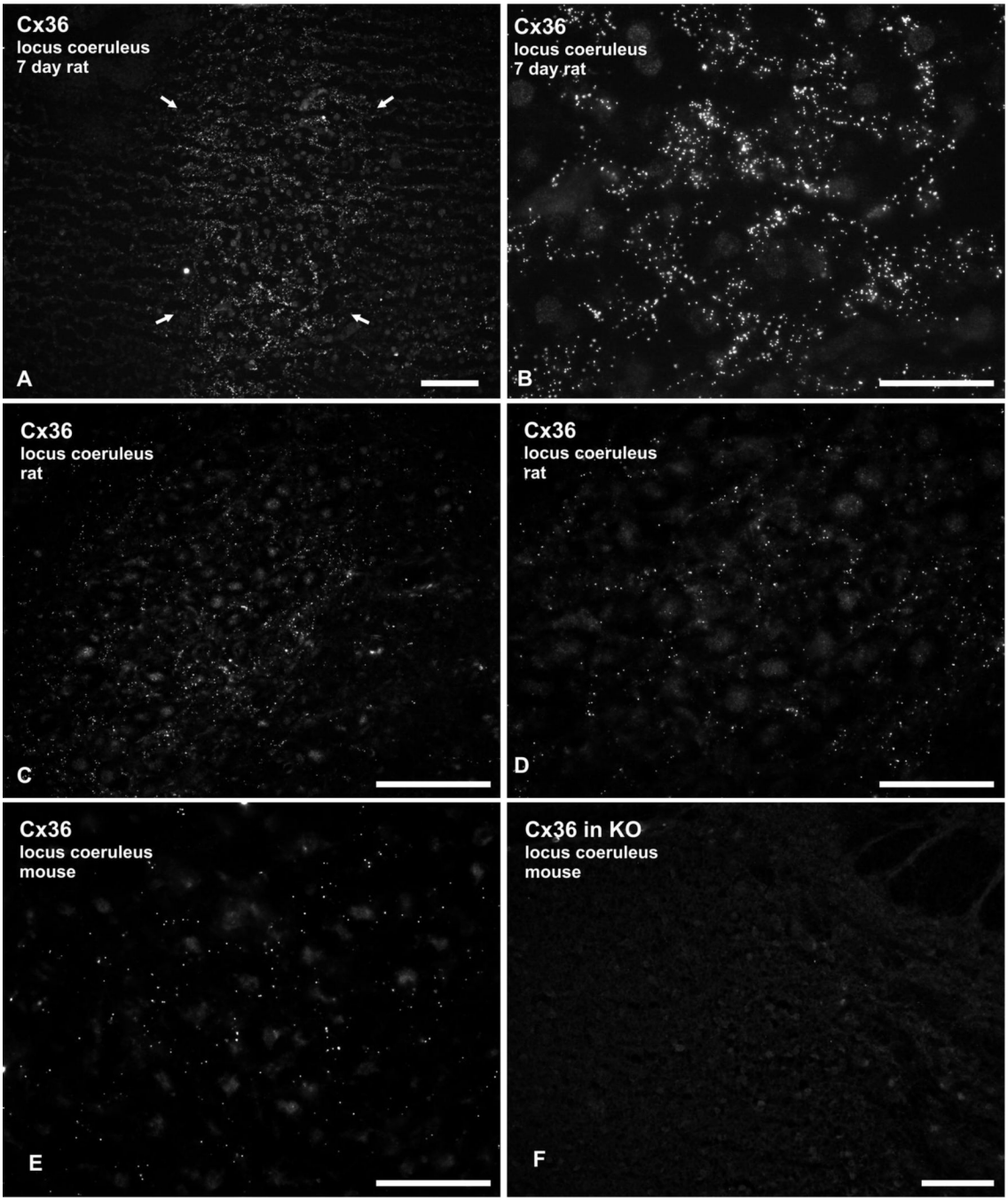

Fig 1.

Immunofluorescence labeling of Cx36 in P7 and adult rodent LC. (A) Low and (B) high magnification micrographs showing Cx36 in rat LC at postnatal day 7. Labeling is dense within the LC (A, arrows) and very sparse in immediately surrounding regions. Immunofluorescence consisting of Cx36-positive puncta are seen distributed among LC neurons exhibiting weak nuclear background fluorescence (B). (C,D) Adult rat LC showing moderate punctate labeling for Cx36, as seen at low (C) and higher (D) magnification. Large neuronal somata among Cx36-positive puncta display weak background fluorescence. (E,F) Micrographs showing labeling of Cx36 in the LC of adult wild-type mouse, and absence of labeling in a similar field of the LC from Cx36 knockout (KO) mouse. Scale bars: A,C,F 100 μm; B,D,E, 50 μm.

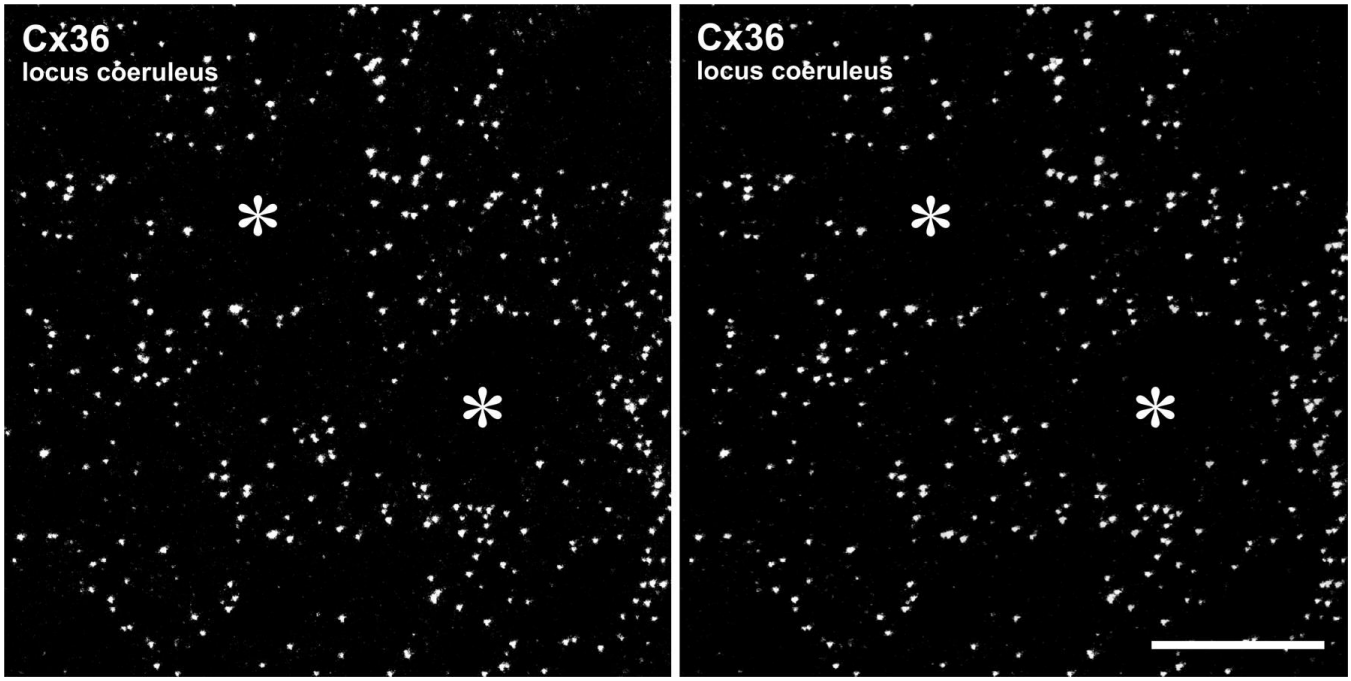

Fig 2.

Laser scanning confocal micrographs of immunolabeling for Cx36 in adult rat LC. (A1, A2) Images showing the same field of a z-stack consisting of 33 scans, with the right image (A2) tilted 7° in the x-y plane to yield a stereo pair. Circular areas devoid of Cx36-positive puncta (asterisks) represent locations of neuronal somata. Scale bar: 20 μm.

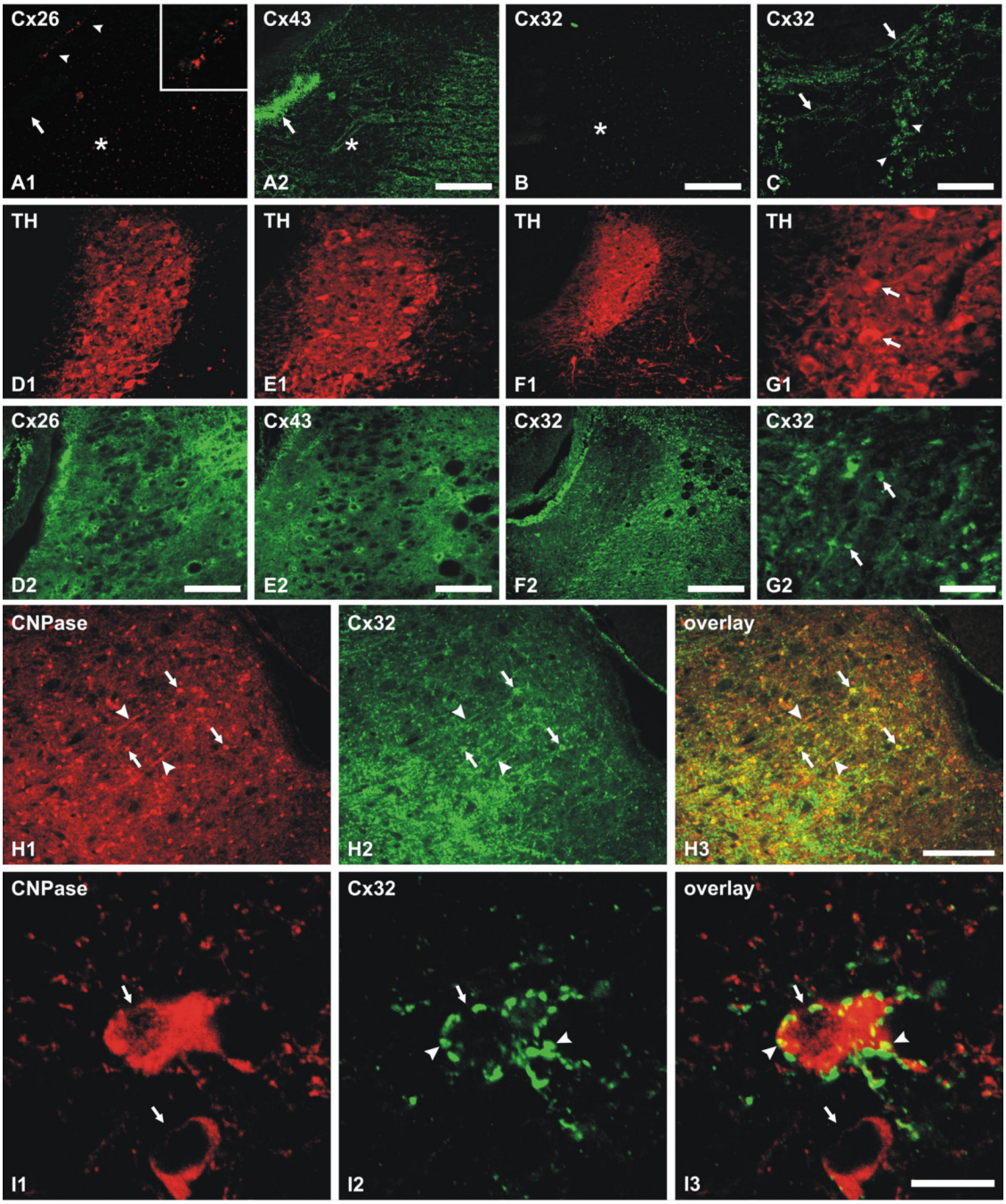

Fig 3.

Immunofluorescence localization of connexins in rat LC. (A) Double immunofluorescence of the same field from 7 day postnatal rat showing absence of labeling for Cx26 in the LC (A1), and moderate labeling for Cx43 in the LC and surrounding regions, including ependyma (A2, arrow). Arrows indicate location of the fourth ventricle, asterisks mark the center of the LC, and arrowheads (A1) show positive labeling for Cx26 within leptomeninges (arrowheads, shown at higher magnification in inset). (B,C) Micrographs showing absence of labeling for Cx32 within the LC (B, asterisk), and, in the same section, positive labeling for Cx32 in oligodendrocytes (C, arrowheads) and sparse myelinated fibers (C, arrows) at a midline brainstem level. D-F: Double immunofluorescence in adult rat showing localization of TH-

positive neurons (D1, E1 and F1) in relation to dense labeling for Cx26 (D1, D2, same field) and Cx43 (E1, E2, same field), and sparse labeling for Cx32 (F1, F2, same field) in the LC. (G) Higher magnification double labeling in the same field showing large TH-positive neurons (G1, arrows) and, in the same field, sparsely distributed smaller Cx32-positive cells (G2, arrows) within the LC. H: Double immunofluorescence labeling of CNPase (H1) and Cx32 (H2) in a region just rostral to the LC showing abundant CNPase and Cx32 co-localization at oligodendrocyte somata (arrows) and myelinated fibers (arrowheads), as seen in overlay (H3). (I) Confocal double immunofluorescence labeling of CNPase-positive oligodendrocyte somata (I1, arrows) within the LC, one of which is surrounded by Cx32-positive puncta (I2, arrowheads), as seen in overlay (I3). Scale bars: A,B,F 200 μm; C,D,E, 100 μm; G, 50 μm; H, 150 μm; I, 10 μm.

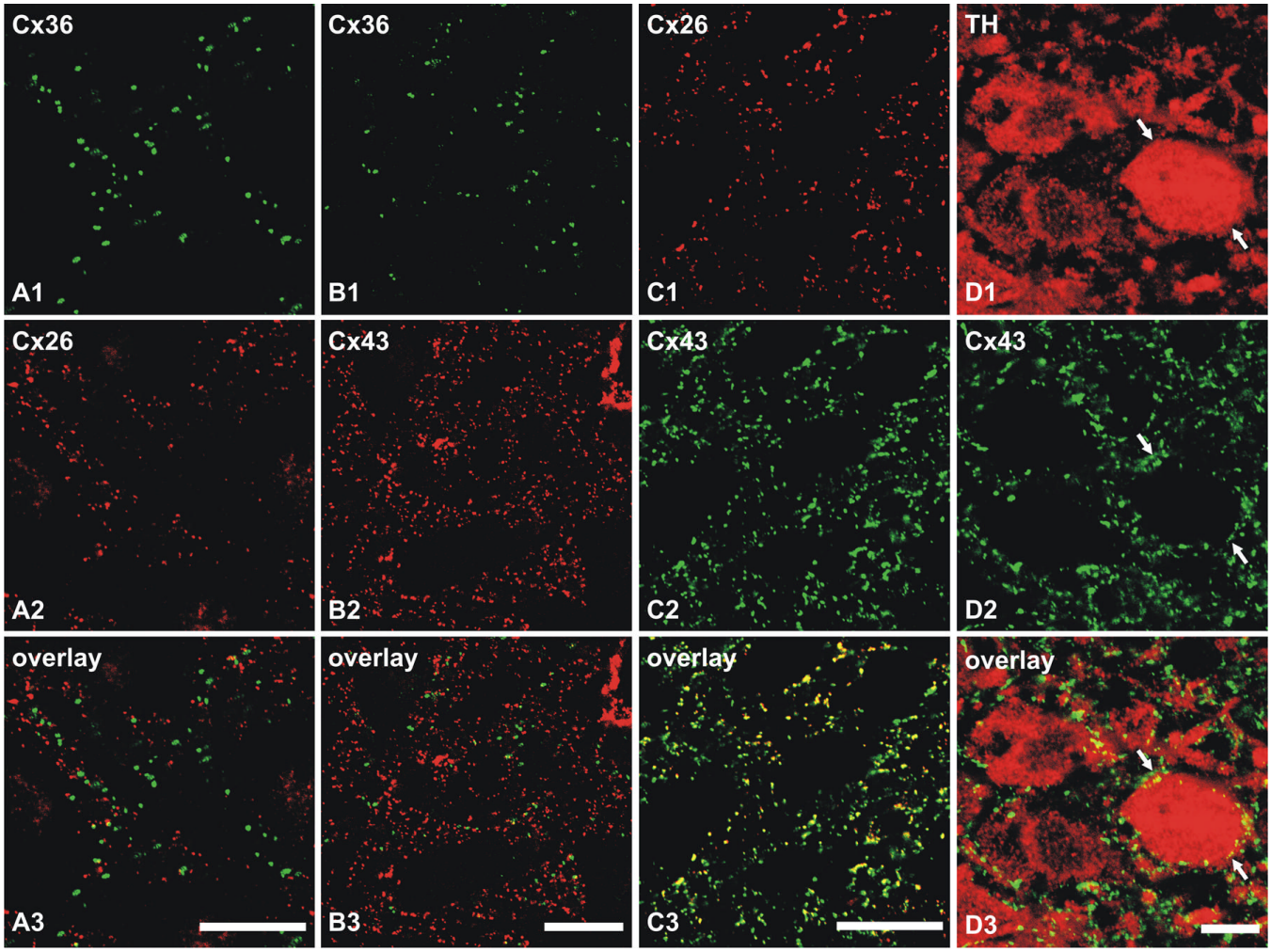

Fig 4.

Confocal double immunofluorescence combinations of labeling for Cx26, Cx36 and Cx43 in rat LC. (A) Double labeling in the same field showing lack of co-localization of Cx36-positive puncta (A1) with Cx26-positive puncta (A2), as seen in overlay (A3). (B) Double labeling in the same field showing lack of co-localization of Cx36-positive puncta (B1) with Cx43-positive puncta (B2), as seen in overlay (B3). (C) Double labeling in the same field showing nearly all Cx26-positive puncta (C1) co-localized with Cx43-positive puncta (C2) but not all Cx43 co-localized with Cx26, as seen by yellow in overlay (C3). (D) High magnification confocal double immunofluorescence showing TH-positive neurons within the LC (D1, arrows) and, in the same field, the close proximity of Cx43-positive puncta (D2, arrows) surrounding these neurons, as seen in overlay (D3). Scale bars: A-C, 20 μm; D, 10 μm.

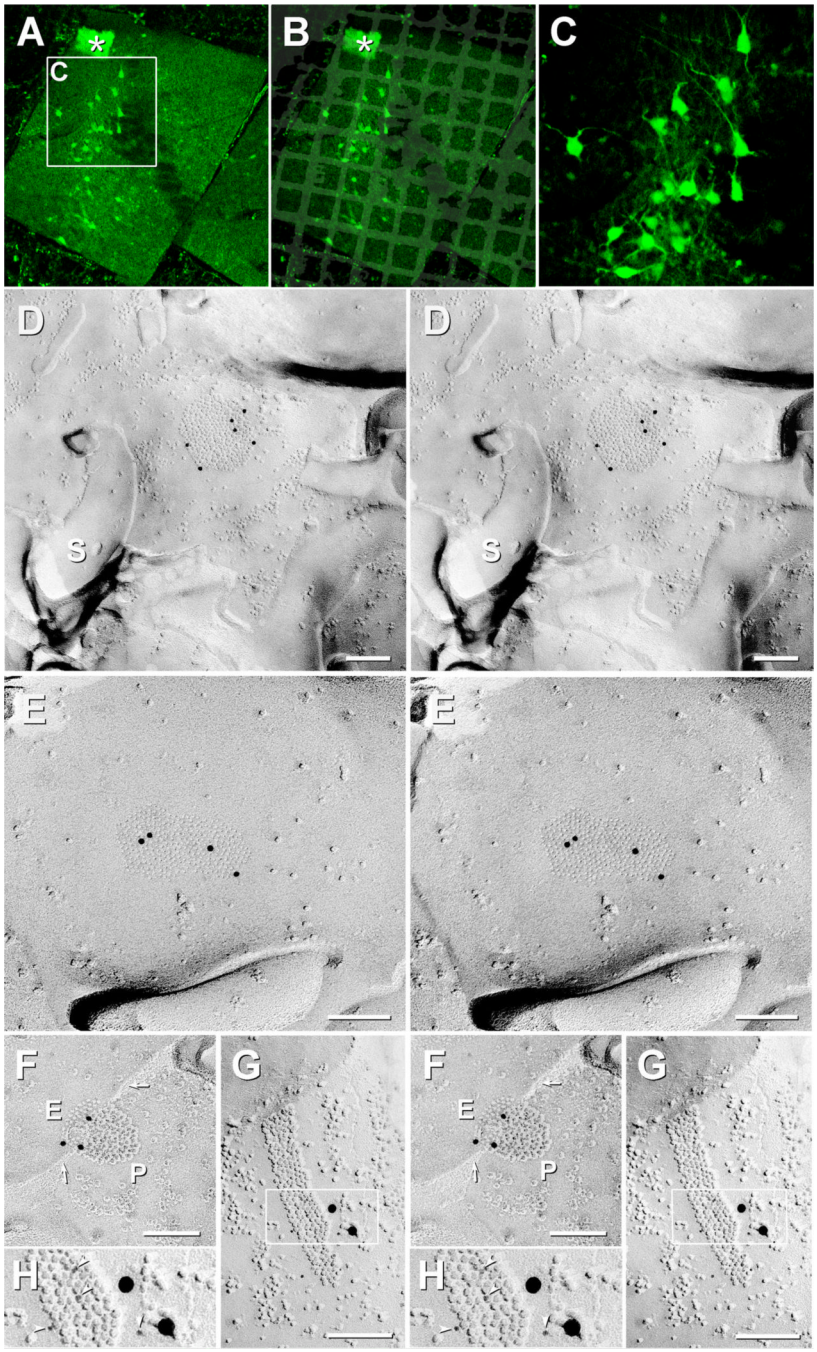

Fig 5.

Localization of LC using P21 mice having EGFP-labeled LC neurons, and demonstration of Cx36-immunogold-labeled gap junctions in neurons of P14 rat LC. A) Fluorescence image of sections of LC on gold "index" TEM grid. Inscribed area shown at higher magnification in C. Ependymocytes of the 4th ventricle (*), with their abundant cilia and microvilli, served as an additional anatomical marker at the edge of most replicas. B) Overlay showing exact location of TEM grid, bonded in Lexan to the freeze-fractured slice of LC. C) Higher magnification image showing individual EGFP neurons and their multiple dendrites. D-H) Neuronal gap junctions found in P14 rat locus coeruleus after double-labeling for Cx26+Cx36 (D-F) or Cx32 +Cx36 (G,H) using three sizes of gold beads for the two primary antibodies. All connexons

are in hexagonal crystalline array. (D) Medium-diameter dendrite P-face with gap junction consisting of ca. 290 connexon IMPs that are labeled for Cx36 by six 12-nm gold beads (LE = 1:50). Cx26 was labeled by 6-nm and 18-nm gold beads (none present). *S*, spine from nearby dendrite. (E) Approximately 280 E-face pits labeled for Cx36 by four 12-nm gold beads (LE = 1:70). (F) Gap junction with step from P-face (P) to E-face (E); ca. 115 connexons labeled by three 12-nm gold beads (LE = 1:40). Arrows, narrowing of extracellular space at contact point of gap junction. (G,H) Portion of neuronal gap junction in P14 LC after double-labeling for Cx36+Cx32. The 219 P-face connexons are labeled by nine 6-nm gold beads and two 18-nm gold beads (LE = 1:20) and for Cx32 (12-nm gold beads, none present). (H) Higher magnification, reverse stereoscopic image of the inscribed area in (G). *Arrowheads*, 6-nm gold beads, which appear “on top” of the intaglio view of the replica.
Scale bars in all FRILimages are 0.1μm unless otherwise designated.

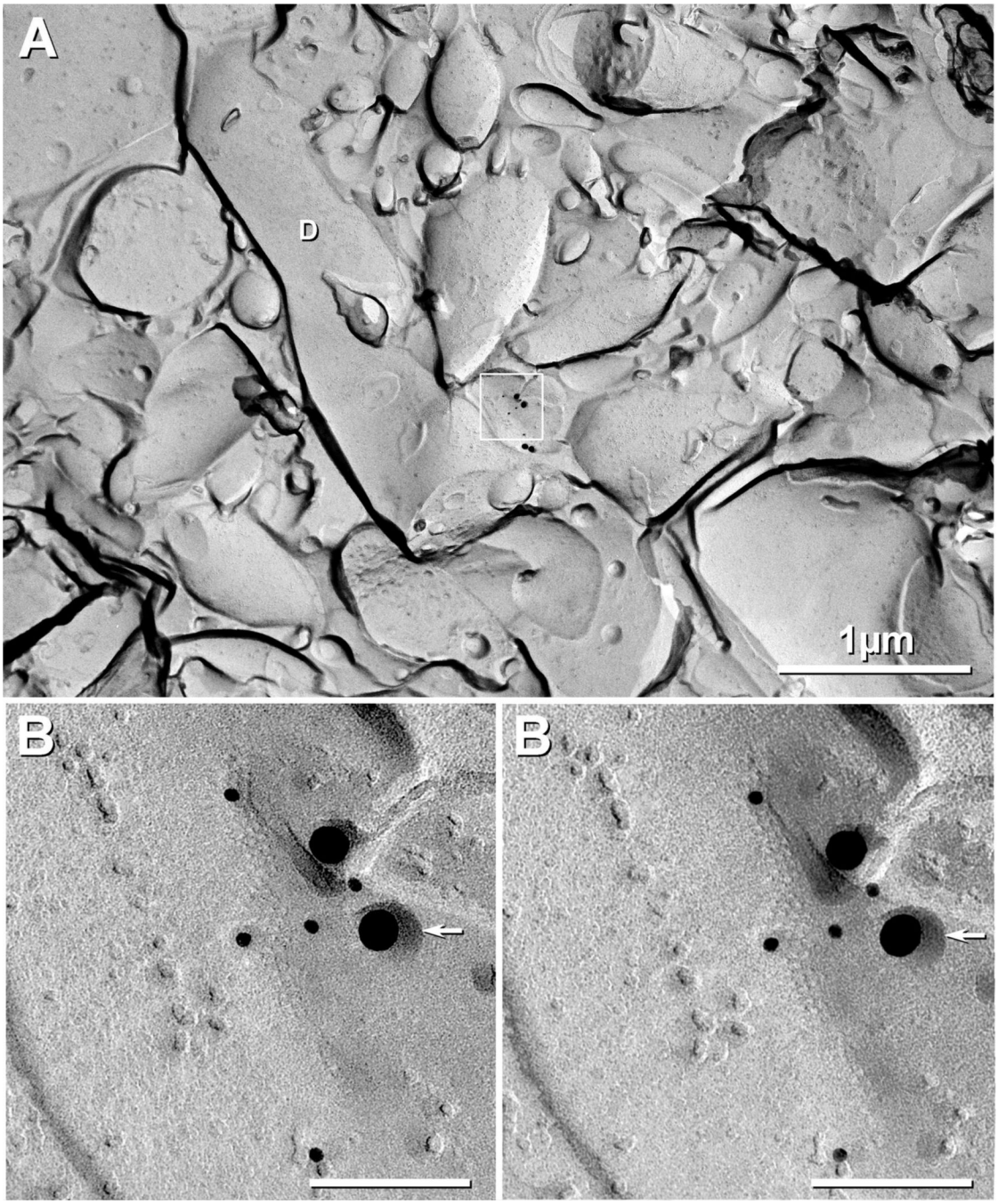

Fig 6.

Cx36-labeled neuronal "ribbon" gap junction in LC of P21 EGFP mouse. A) Low magnification overview of 1-μm diameter dendrite with small synaptic contact containing gap junction (inscribed box). D, dendrite. B) At higher magnification, this neuronal gap junction, which consists of ca. 80 connexons, is labeled for Cx36 (five 12-nm and two 30-nm gold beads; LE = 1:10), but Cx26 (6-nm and 18-nm gold beads, none present) was not detected. At the lower edge of the box in (A), in the area not shadowed by platinum (and hence where connexon pits would not be resolvable), are two additional 30-nm gold beads for Cx36. Although these were located beyond the normal 28-nm radius of labeling for immunogold (Kamasawa et al., 2006), because of close proximity and extremely low background, they are presumed to

represent labeling of detaching membrane blebs created during SDS washing (Kamasawa et al., 2006). Arrowhead, secondary stabilizing carbon coat applied prior to removing the Lexan support film (see Methods).

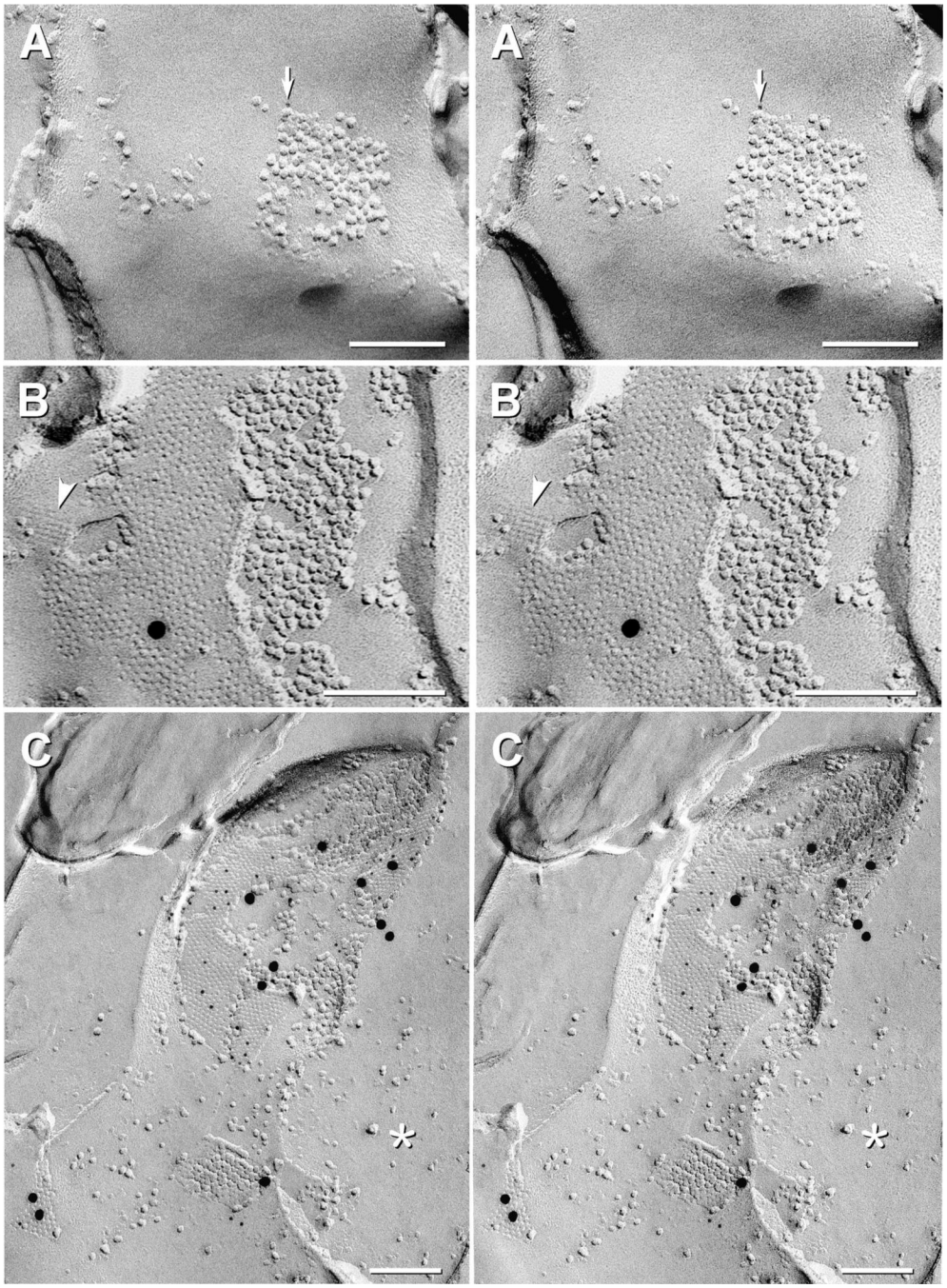

Fig 7.

Rare and weak labeling for Cx32 and Cx26 in oligodendrocyte and astrocyte gap junctions at P14 and P21, but strong labeling for Cx26 in pia mater at P28 using the same primary antibody to Cx26 and the same 6-nm and 18-nm secondary antibodies. (A) Stereoscopic image of small gap junction in the edge of a “reciprocal patch” (Nagy et al., 2001) on the outer surface of myelin. It was weakly labeled for Cx32 by one 6-nm gold bead (arrow) but not for Cx36 (12-nm; none present). (B) Stereoscopic image of a large gap junction between astrocyte processes in P21 LC. The gap junction was either very weakly labeled for Cx26 (6-nm gold [none present] and 18-nm gold [one present] or was not labeled at all. (Background was extremely low, so the single gold bead served as a “flag” to find gap junctions, and thus, was considered to

represent a “probable” label.) Arrowhead, E-face imprint of AQP4 array. (C) Stereoscopic image of three Cx26-labeled gap junctions (44 6-nm and 11 18-nm gold beads) linking cells of the pia mater surrounding P28 rat cerebellum, confirming high labeling efficiency for primary and secondary antibodies used in companion experiments on P14 and P21 LC. *, cytoplasm.

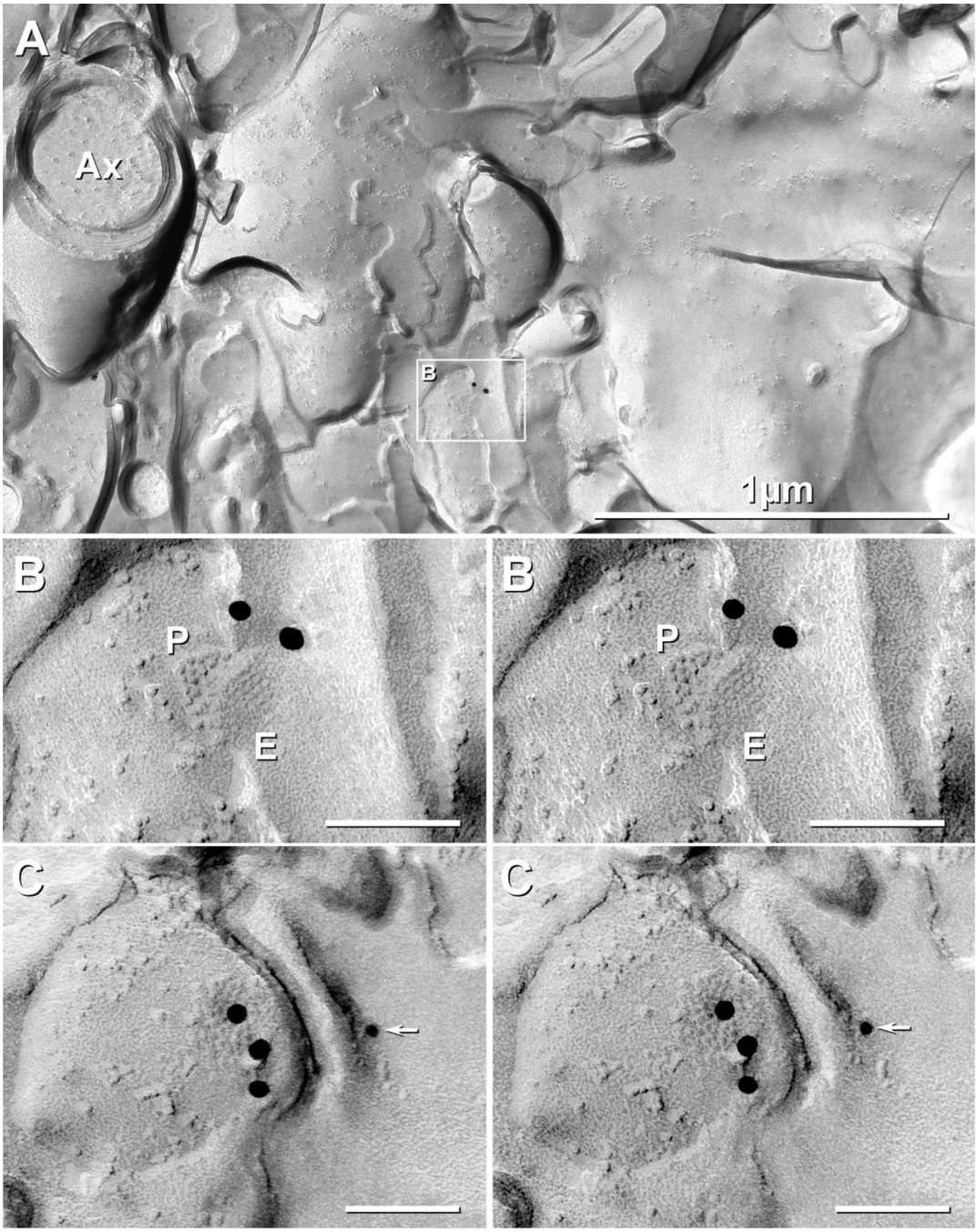

Fig 8.

Cx36-immunogold-labeled gap junctions in P28 (adult) rat LC. (A) At low magnification, a few myelinated axons (Ax) are seen to pass through the nucleus of the LC. This sample was triple-labeled for Cx36 (two 18-nm gold beads) and for Cx32 and Cx47 (6-nm and 12-nm gold beads; none present on neuronal gap junctions). However, Cx32 and Cx47 were abundant in oligodendrocyte gap junctions (see Fig. 9A-C). Inscribed area in (A) is enlarged as (B). Extremely low background (A) allowed detection of gap junctions consisting of ca. 46 and 48 connexons labeled by two (B) and three (C) 18-nm gold beads (LE ≈1:20). (C) Stereoscopic image of electrical synapse shared with dendrite reveals that one additional 12-nm gold bead, potentially representing labeling for Cx47 (arrow), was on the upper surface (Lexan-coated,

non-tissue side) of the replica, thereby confirming that the gold bead does not represent specific labeling. P, P-face; E, E-face.

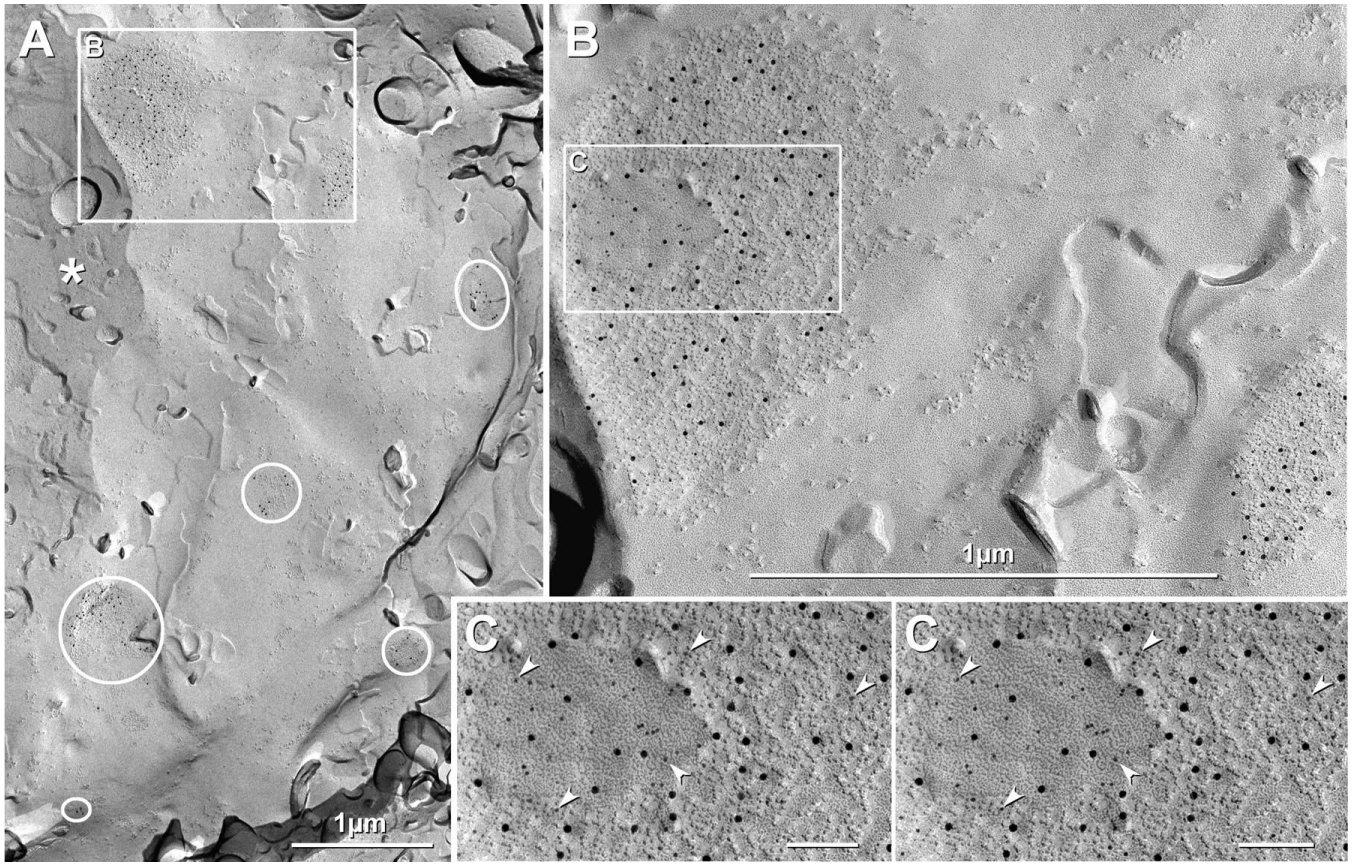

Fig 9.

Oligodendrocyte gap junctions in adult LC triple-labeled for Cx32, Cx47 and Cx36. (A) Seven gap junctions (ovals and square) on oligodendrocyte soma in adult rat locus coeruleus labeled for Cx32 by >100 6-nm gold beads and for Cx47 by >85 12-nm gold beads. (B,C) Progressively higher magnification images of gap junction in inscribed box in (A). (C) Reverse stereoscopic image of a portion of the gap junction within inscribed box in (B), revealing the high density of 6-nm gold beads labeling Cx32. Arrowheads, 6-nm gold beads for Cx32. Gold beads for Cx36 (18-nm gold beads) are not present on oligodendrocyte gap junctions but are on neuronal gap junctions in this same replica (Fig. 8). *, oligodendrocyte cytoplasm.

Table 1

Antibodies used for immunohistochemistry and FRIL

Antibody	Type	Species	Epitope; Designation*	Dilution**	Source; Reference
Cx26	monoclonal	mouse	c-terminus; 33−5800	2 μg/ml, 10 μg/ml	Invitrogen/Zymed
Cx26	polyclonal	rabbit	c-terminus; 51−2800	2 μg/ml, 10 μg/ml	Invitrogen/Zymed
Cx32	monoclonal	mouse	c-terminus; 35−8900	2 μg/ml	Invitrogen/Zymed
Cx32	monoclonal	mouse	aa 95−125; MAB3069	10 μg/ml	Chemicon
Cx32	polyclonal	rabbit	cytoplasmic loop; 71−0600	10 μg/ml	Invitrogen/Zymed
Cx32	polyclonal	rabbit	c-terminus; 34−5700	2 μg/ml	Invitrogen/Zymed
Cx36	monoclonal	mouse	c-terminus; 39−4200	3 μg/ml	Invitrogen/Zymed
Cx36	polyclonal	rabbit	c-terminus; 36−4600	3 μg/ml, 10 μg/ml	Invitrogen/Zymed
Cx36	monoclonal	mouse	c-terminus; 37−4600	10 μg/ml	Invitrogen/Zymed
Cx43	monoclonal	mouse	c-terminus; 35−5000	2 μg/ml	Invitrogen/Zymed
Cx43	polyclonal	rabbit	aa 346−363; 18A	1:5000	Yamamoto et al., 1990a
Cx43	polyclonal	rabbit	c-terminus; 71−0700	2 μg/ml	Invitrogen/Zymed
Cx47	polyclonal	rabbit	c-terminus; 36−4700	2 μg/ml, 10 μg/ml	Invitrogen/Zymed
Cx47	monoclonal	mouse	c-terminus; 37−4500	10 μg/ml	Invitrogen/Zymed
CNPase	monoclonal	mouse	whole protein	1:5000	Sternberger Monoclonals
TH	polyclonal	rabbit	whole protein	1:400	Eugene Tech

* aa, amino acids

** For FRIL, dilutions were ca. 10 μg/ml.

Table 2

Numbers of replicas examined, ages of animals, connexins examined, areas examined, and number of labeled gap junctions found for each connexin in each cell type.

Age (animal)	Connexin / # replicas	Area in μm^2	# GJs (cell type)	# GJ per 100,000 μm^2
P7-P14 (rat)	Cx26 / 3	24,300	0	0
	Cx32 / 5	67,800	1 (oligo)	1.4
			0 (neuron)	0
	Cx36 / 7	29,300	6 (neuron)	20*
P21 (mouse)	Cx26 / 1	1,000	1 (astro)	*
	Cx32 / 2	43,600	1 (oligo)	2
			0 (neuron)	0
	Cx36 / 2	28,000	1 (neuron)	3.6*
P28 (rat and mouse)	Cx26 / 1	(cerebellum)	(lepto)	NA
	Cx32 / 2	16,900	>20 (oligo)	118#
	Cx36 / 2	9,100	2 (neuron)	22*

* Insufficient area examined / insufficient number of gap junctions for valid calculation.

Highly variable because fractures of individual somata frequently expose dozens of gap junctions, rather than the single gap junctions usually seen in neurons.